REVIEW

Check for updates

Advances in metal–organic frameworks for water remediation applications

Seema Lal, [ID] [a] Parul Singh, [a] Anchal Singhal, [b] Sanjay Kumar, [ID] [a] Ajay Pratap Singh Gahlot, [ID] [c] Namita Gandhi [a] and Pratibha Kumari [ID] *[a]

Rapid industrialization and agricultural development have resulted in the accumulation of a variety of harmful contaminants in water resources. Thus, various approaches such as adsorption, photocatalytic degradation and methods for sensing water contaminants have been developed to solve the problem of water pollution. Metal–organic frameworks (MOFs) are a class of coordination networks comprising organic-inorganic hybrid porous materials having organic ligands attached to inorganic metal ions/ clusters *via* coordination bonds. MOFs represent an emerging class of materials for application in water remediation owing to their versatile structural and chemical characteristics, such as well-ordered porous structures, large specific surface area, structural diversity, and tunable sites. The present review is focused on recent advances in various MOFs for application in water remediation *via* the adsorption and photocatalytic degradation of water contaminants. The sensing of water pollutants using MOFs *via* different approaches, such as luminescence, electrochemical, colorimetric, and surface-enhanced Raman spectroscopic techniques, is also discussed. The high porosity and chemical tunability of MOFs are the main driving forces for their widespread applications, which have huge potential for their commercial use.

1. Introduction

Water is essential for life. According to the 2021 World Water Development Report published by UNESCO, global freshwater consumption has increased six-fold over this century and has been increasing by about 1% annually since the 1980s.[1] However, with the increasing utilization of water, maintaining the water quality has become a major challenge. In recent times, water pollution has been a serious threat to mankind on the global level. Agricultural production, industrialization, and urban life have a significant impact on the quality of water bodies, posing a threat to human health and sustainable social development.[2] According to a survey, around 2 million tons of wastewater and other effluents are drained into water bodies daily without any prior treatment. Furthermore, water pollution is more pronounced in developing countries, where wastewater treatment facilities and sanitation are obstinately lacking.

Water pollution regulation has emerged as an important environmental challenge, hence attracting increasing interest from many scientists globally. Various processes have been developed for water decontamination, including adsorption, sedimentation, filtration, precipitation, reverse osmosis,

flocculation, and degasification. Among them, adsorption has attracted widespread attention and preferred over conventional methods owing to its higher efficacy and recovery processes.[3] Another rapidly developing approach for water treatment is the photodegradation of pollutants. Besides, the sensing of water contaminants is also a crucial step in the water treatment process. Accordingly, optimum sensing techniques in combination with efficient adsorption and photocatalytic degradation methods have great potential to solve the problem of water pollution.

MOFs are hybrid crystalline materials, similar to zeolites and aluminophosphates, made of inorganic nodes (such as atoms, chains, and clusters) linked *via* organic linkers (azolates, carboxylates, phosphonates, *etc.*), which can be assembled to form a huge network of polymers with different topologies.[4] The crystalline structure of MOFs makes their structural characterization simple. To date, many different classes of MOFs have been reported in the literature, such as iso-reticular metal–organic frameworks (IRMOFs), metal–organic polyhedra (MOP), zeolitic imidazole frameworks (ZIFs), porous metal organic frameworks (PMOFs), coordination polymers (CPs), porous coordination polymers (PCPs), and microporous metal organic frameworks (MMOFs). The synthesis of these materials involves the formation of metal–organic complexes, followed by their self-assembly into a desired framework structure. To date, a variety of synthesis protocols has been developed, including solution-based methods, such as hydrothermal, solvothermal, and

[a]Department of Chemistry, Deshbandhu College, University of Delhi, New Delhi, India
[b]Department of Chemistry, St. Joseph's College, Bengaluru, Karnataka, India
[c]Department of Physics, Deshbandhu College, University of Delhi, New Delhi, India.
E-mail: pkumari@db.du.ac.in

precipitation synthesis, as well as gas-phase methods, such as aerosol-assisted synthesis and inert gas condensation. The choice of synthesis method depends on the desired properties of the final material and the complexity of the framework structure. MOFs can be modified post-synthetically to impart affinity for specific contaminants.[5] To obtain different morphologies, variable crystal structures, MOF membranes, MOF thin films, various modifications are implemented in existing methodologies.[6,7] Fig. 1A presents the preparation strategies, obtained morphologies, sizes, and fabrication of the different MOF materials used in water remediation applications. These MOFs can be used as efficient materials for adsorption, photodegradation, and sensing of water contaminants (Fig. 1B).

Presently, MOFs are attracting increasing interest in a variety of fields due to their diverse applications including catalysis,[8] biocatalysis,[9] sensing,[10] adsorption,[11] light harvesting,[12] fuel cells,[13] separation,[14] and drug delivery.[15] Among them, their application is highly recommended as one of the modern techniques for wastewater decontamination due to their remarkable properties such as high surface area, large pore volume, abundant active sites to adsorb and desorb contaminants, high sorption capacity, good stability in water, tunable host–guest interactions and feasible tailoring to achieve shape selectivity. The most common classes of MOFs that are applied in water remediation are represented in Fig. 2. MOFs can be shaped into different forms such as pellets, monoliths, columns, and membranes suitable for pollutant removal devices.[16] Besides the adsorption of pollutants, MOFs have been used for wastewater decontamination employing catalytic processes.[4] This high demand for MOFs in water decontamination is attributed their high tunability and convenient *in situ* and post-synthetic modification together with their stability in
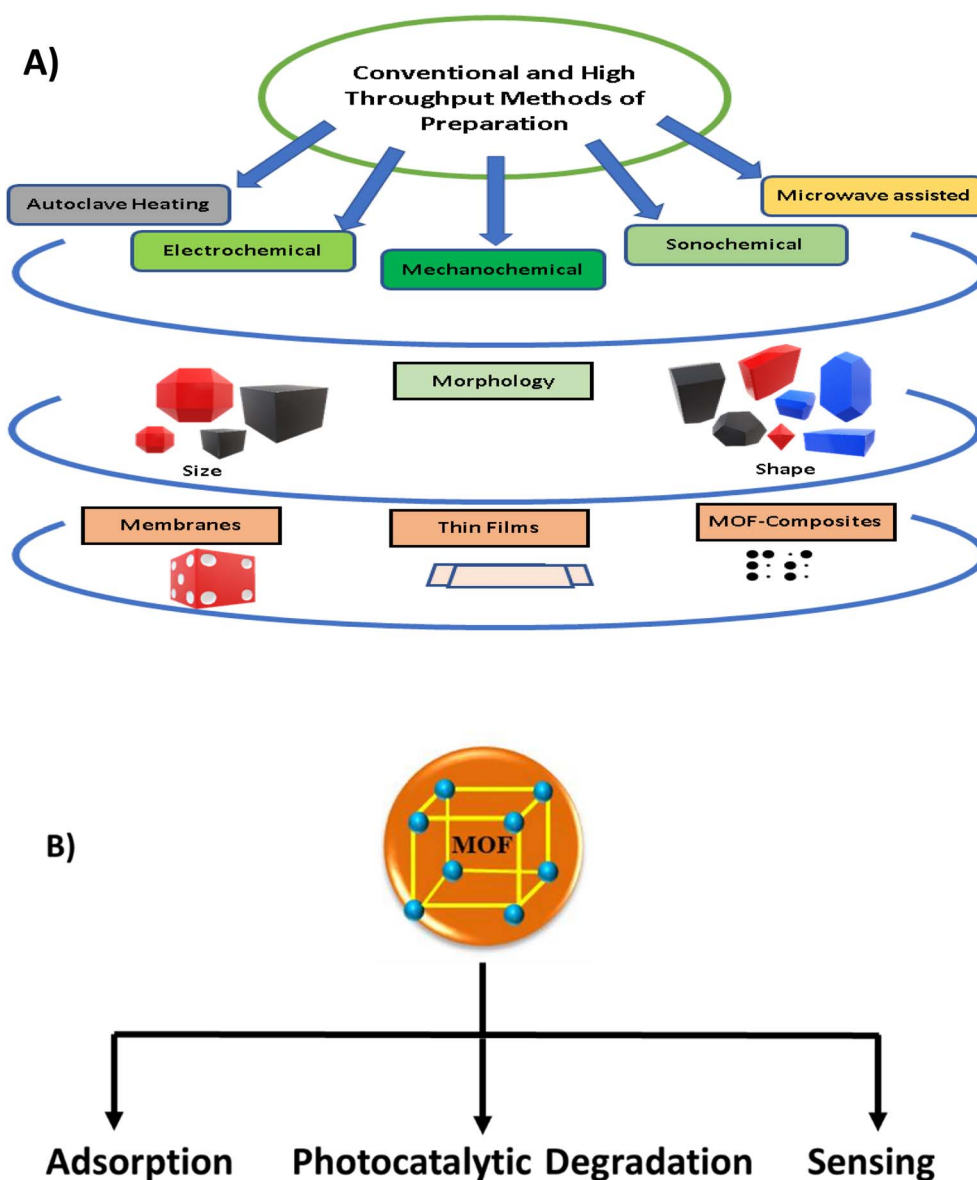

Fig. 1 (A) Different morphologies and methods for the fabrication of MOFs and (B) role played by MOFs in water treatment approaches.

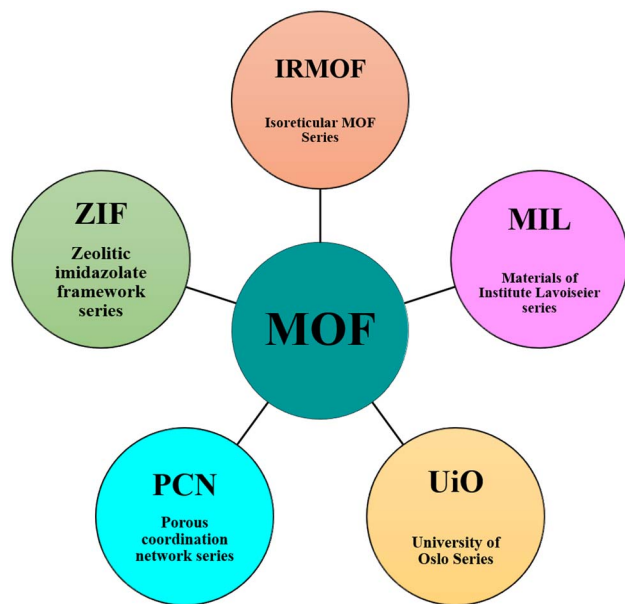© 2024 The Author(s). Published by the Royal Society of Chemistry

Fig. 2 Different types of MOFs used for water remediation applications.

water. Usually, the fundamental source of the high chemical and hydrolytic stability of MOFs is their strong metal–ligand coordination bonds, resulting in thermodynamically stable products or significant steric shielding of the metal–ligand bond (kinetic control product), which prevents their hydrolysis.[17] Metal-carboxylates, metal-azolates, and metal-hydrophobic functionalization are the common chemical configurations that endow MOFs with chemical and hydrolytic stability.[18] To date, various cationic and anionic water-soluble MOFs have been reported in the literature that show efficient anion sensitivity, and hence used to remove ionic pollutants selectively based on their size, charge, and mass ratio.

MOFs can be tailored to possess specific pore sizes, allowing them to adsorb specific molecules or contaminants from water. Furthermore, MOFs can be reused several times without losing their adsorption capacity or efficiency, making them cost-effective. These properties of MOFs make them versatile for the removal of water contaminants through different mechanisms. Recently, Thakur and team highlighted the synthesis and active mechanism of function of advanced MOFs as adsorbents for the removal of hazardous pollutants under different environmental conditions.[19] Xia and group developed three Zr-based MOFs with different topologies and pore sizes for the removal of tetracycline and studied their kinetics and mechanism in detail.[20]

MOFs have developed into next-generation utility materials due to their versatility. Furthermore, due to their structural and efficient tunability, MOFs are the most interesting materials for water contaminant sensing.[21] These porous materials have been demonstrated to be a new tool in the area of sensing different types of water contaminants due to their outstanding chemical stability and a wide variety of functional groups. The numerous functional groups present in MOFs dictate the selective approach for sensing. The affinity of the functional groups and some chemical reactions of MOFs with contaminants are

mainly responsible for their selective sensing. Recently, Ghosh and co-workers developed new task-specific porous and crystalline MOFs, which exhibited remarkable selectivity as sensory probes.[22] Furthermore, they developed a method for specific cyanide ion (CN^-) detoxification in aqueous medium employing bio-MOF-1, possessing the molecular formula $[Zn_8(ad)_4(BPDC)_6O \cdot 2Me_2NH_2]G$ (G= water, DMF) with a cationic dye (DAAC) (3,6-diaminoacridinium cation) embedded in it. This specific MOF showed the remarkable property of selectively removing CN^- ions because of the strong ability of the dye to undergo a Michael addition-type reaction.

The performance of MOFs in water remediation is highly influenced by their chemical stability under different conditions. The chemical stability of MOFs refers to their ability to maintain their long-ranged ordered structure in a certain chemical environment. Alternatively, the strength of the coordinate bonds of MOFs is believed to be responsible for their thermodynamic stability. Specifically, it can be explained as the resistance of MOFs to chemical treatments such as water, acid, alkali, and salt solutions to maintain their framework integrity and porosity. During these treatments, the instability of MOFs is attributed to the break of their metal–ligand bond.[23] The chemical stability of MOFs depends on their intrinsic structures (internal factors), including the charge density of their metal ions, number of connections of metal ions/clusters, basicity, configuration and hydrophobicity of their ligands. The chemical factors that affect the stability of MOFs include their bonding strength, ligand design, metal ion, pH and chemical environment, and thermal stability. Therefore, the stability of MOFs, especially their water stability is crucial for their wide range of applications including water treatment.

The exquisite combination of feasible pore architecture alteration and hydrolytic stability of MOFs make them versatile sorbent tools with shape and sensing selectivity for the removal of hazardous and emerging pollutants in aqueous medium. This review will assist researchers in gaining a thorough understanding of the interactions between MOFs and various pollutants including metal ions, pesticides, pharmaceutical compounds, and dyes, as well as strategies for designing and synthesizing MOF-based materials as high-performance adsorbents and sensors for environmental pollution management.[24] Herein, we demonstrate the recent advances in the application of MOFs in various aspects of water treatment including adsorption, photodegradation, and sensing of pollutants. However, MOFs have been demonstrated to be unsuitable for utilization under harsh conditions due to their stability issues. In this case, new approaches have developed to fabricate stable and efficient MOFs for commercial applications.

2. Water-stable MOFs for water remediation applications

MOF materials are conjugated clusters of metal ions and organic linkers, which impart high porosity to their structure. Furthermore, the easy tunability of their pore size and shape makes them fascinating for various applications. A range of

mesoporous to microporous structures can be easily achieved by adopting different methodologies. The ultimate goal of MOF synthesis is to establish conditions which inorganic building blocks are formed without the decomposition of the organic linkers. Also, the nucleation and growth of the desired phase should ensure crystallization.[25] The synthetic methodology of MOF structures evolved from a diverse historical background, where the synthesis of porous materials was attempted using building blocks of inorganic and organic moieties under mild reaction conditions.[26] Later stages include the use of organic moieties as linkers and as a part of the reacting species instead of structure-directing agents. This included the use of elevated temperature during the reaction procedures, and hence many groups employed methodologies based on reaction temperature and reactor.[27] Ghosh *et al.*[28] reported the water stability of neutral nitrogen-donor ligand-based MOFs, which exhibited high sensing ability.

It is necessary to address the issue of the poor water stability MOF materials to guarantee their desired application in water. Wang *et al.*[29] defined water-stable MOFs as a category of MOFs that exhibit no structural damage and maintain their functional stability when exposed to water. The water stability of MOFs involves assessing the extent of changes in their typical chemical characteristics after exposure to an aqueous environment. Internal and external operational factors are two major categories that can be used to categorize the factors that influence the water stability of MOFs. Internal factors include crystallinity, pore surface hydrophobicity, and porosity. Other internal parameters include the strength of the metal–organic coordination bonds and metal–ligand coordination geometry. Examples of external influences are temperature, pH, and humidity.[30]

2.1 Factors influencing the water stability of MOFs

The water stability of MOFs is influenced by several factors, including thermodynamic, kinetic, and environmental factors. The thermodynamic factor primarily depends on the strength of the coordination bonds in MOFs. When unstable MOFs come into contact with water, hydrolysis reactions occur, leading to the breakage of their coordination bonds and the occupation of their central metal ions by other coordination molecules. This results in the collapse of the MOF structure and loss of its permanent pores. The strength of coordination bonds can be analyzed theoretically based on Pearson's hard/soft acid/base (HSAB) principle, which considers the orbital radius and polarity of the metal cations and organic ligands. Stronger bonding strength is observed when the main orbital radius and polarity of the metal ions and ligands are close and the valence state of the metal cation is high and its radius is small. The interaction mechanism between water and MOFs has been extensively studied due to their potential applications in water sorption-related fields such as moisture control, refrigeration, heat storage, dehydration, desiccation, and water harvesting. Water-stable MOFs possess strong coordination bonds and spatial resistance to prevent structural damage caused by water molecules.

Water stability in MOFs encompasses various aspects that are vital for their practical applications. Understanding and enhancing the water stability of MOFs are crucial to maintaining their structural integrity and functional performance in aqueous or high-humidity conditions. One important aspect of water stability of MOFs is their hydrolysis. The thermodynamics and kinetics of MOF hydrolysis play a significant role in determining their long-term stability when exposed to water.[31] Furthermore, the collapse of the MOF pores due to the capillary forces exerted by water is another challenge that affects their water stability. Preventing pore collapse is crucial for applications such as water adsorption, corrosive gas adsorption, and other processes reliant on maintaining the porosity and crystallinity of MOFs. Techniques such as solvent exchange with nonpolar solvents or supercritical CO_2 can help overcome this challenge and enhance the water stability of MOFs. Enhancing the water stability of MOFs is important for various applications, including water contaminant detection and removal, biomedicine, proton conduction, and catalysis. Thus, by ensuring the structural integrity, crystallinity, and porosity of MOFs in aqueous or high-humidity environments, their performance and reliability can be significantly improved.[32,33]

2.1.1 Thermodynamic factors. To achieve MOFs with thermodynamic stability, it is necessary to consider several parameters, notably to ensure that the irreversible breaking of bonds by water attack is thermodynamically unfavorable. This is demonstrated by the positive value of $G_{hydrolysis}$, which is proportional to the Gibbs free energy of the reactants (MOFs and water) and products (ligand, metal, and water) in the hydrolysis reaction. However, determining $G_{hydrolysis}$ is difficult given that it does not consider the intermediate states. In the hydrolysis reaction, there is a positive entropy change, which is denoted by $S_{hydrolysis}$, as a result of the increasing disorder in the system arising from the disintegration of the MOF. $H_{hydrolysis}$ must be positive in the equation $G_{hydrolysis} = H_{hydrolysis} - TS_{hydrolysis}$, where $H_{hydrolysis}$ represents the enthalpy change. This results in a positive $G_{hydrolysis}$, demonstrating thermodynamic stability and indicating an endothermic hydrolysis process.

For MOFs to be thermodynamically stable, strong coordination bonds must be constructed. These bonds contribute to the overall stability of the MOF structure by making it energetically unfavorable for water to its break bonds. By creating MOFs with robust coordination bonds, scientists can increase their thermodynamic stability and reduce their degradation caused by hydrolysis.[34] The strength of the coordination bond is essentially determined by three factors, *i.e.*, the pK_a of the ligand, the metal charge, and the polarizability match between the metal and ligand based on the hard/soft acid/base concept. Ligands with a higher pK_a display greater basicity and donating capacity, resulting in stronger coordination bonds with metals. This can be generalized by azole ligands, which contain N-donor atoms having a large pK_a and are soft bases, whereas carboxylic acid ligands with a low pK_a are hard bases. It has been reported that MOFs with carboxylate ligands are less stable in water compared to MOFs containing pyrazolate and imidazolium ligands due to the increase in pK_a value from carboxylate

to azole ligands.[35] For example, azolate frameworks with divalent metals, such as ZIF-8 and Zn(1,4-BDP), display high chemical stability even in boiling water, surpassing the stability of most zinc carboxylate MOFs.[36]

The binding strength in MOFs is also affected by the oxidation states and ionic radius of the metal. Higher oxidation states and lower ionic radii result in greater Lewis acidity, which enhances the interaction with basic ligands. MOFs built with high-valence metals such as Zr^{4+}, Ti^{4+}, Cr^{3+}, and Al^{3+} display exceptional stability in aqueous medium. High-valence hard metals bind strongly with oxygen-donating hard bases such as carboxylates and phenolates, while soft late-transition metals bind strongly with nitrogen-donating azolates. Examples of these MOFs include phenolate MOFs produced with high-valence Zr^{4+} metal and phenolate ligands with high pK_a, which satisfy all three requirements and exhibit stability across a wide range of environmental conditions.[37]

2.1.2 Kinetic factors. Enhancing the kinetic water stability of MOFs necessitates the study of the reaction kinetics. Although the thermodynamics of MOF hydrolysis highlights the significance of strengthening the coordination bonds, the kinetics emphasizes boosting the activation energy of the hydrolysis reaction. Several factors influence the kinetics of hydrolysis, including the water–ligand exchange rate, the stability of the metal ion, the rigidity/flexibility of the framework, and the steric hindrance and hydrophobicity of MOFs.

The water–ligand exchange rate of a metal complex has a direct effect on its hydrolysis kinetics, with a quicker exchange rate resulting in more rapid hydrolysis and less stable complexes. Regardless of the ligands, the stability of divalent metal complexes can be represented by the Irving–Williams series, following the order of Pd > Cu > Ni > Co > Zn > Cd > Fe > Mn > Mg. The more stable metal ions will tend to form stable complexes.[38] However, in the case of MOFs, the water–ligand exchange reaction is more complicated due to the constraints of ligand dissociation in their framework, which leads to an increase in the hydrolysis activation energy. Studies have demonstrated that MOFs with stiffer ligands are notably more stable.

Another factor influencing the kinetic stability of MOFs is creating a hydrophobic pore surface and increasing the steric hindrance at the coordination bond. Recently, it was reported that a Zn-based MOF possessed higher water stability due to the incorporation of hydrophobic groups in its framework.[39] Also, MOFs with high coordination numbers show high chemical stability, which is most likely due to the increase in steric hindrance and high degree of stiffness.[40]

2.2 Synthetic approaches to enhance the water stability of MOFs

The synthesis strategies for achieving water-stable MOFs can be broadly categorized into two main approaches, as follows: (1) internal modification and (2) external modification of the MOF structure. Internal modification involves altering the composition of the MOF, such as its metal ions, organic ligands, and metal–ligand coordination geometry, to enhance its thermodynamic stability. Alternatively, external modification involves surface treatments or modifications aimed at improving the kinetic stability of MOFs.

In the case of internal modification, researchers prioritize the selection of metal ions, organic ligands, and the construction of coordination geometries with increased resistance to water-induced deterioration. This method attempts to improve the metal–organic coordination bonds and overall structural strength of MOFs. Alternatively, external modification options involve covering the surface of MOFs with hydrophobic materials or introducing functional groups that enhance the hydrophobicity of their surface. This surface modification helps repel water molecules and reduces their interaction with the MOF, hence enhancing the kinetic stability of the material in the presence of water. In the following subsections, we discuss the processes employed for the synthesis of MOFs, aiming to achieve enhanced stability.

2.2.1 Enhancing the strength of the coordination bond. In an aqueous environment, the water stability of MOFs is influenced by the strength of their metal–organic coordination bonds and the susceptibility of their framework to be attacked by water molecules. Thus, strengthening the metal–organic coordination bonds is a key factor in enhancing the water stability of MOFs.[41] High-valent metal units in MOFs generate larger, more rigid structures that withstand the aqueous environment. Thus, carboxylate-based ligands (hard Lewis bases) and high-valent metal ions (hard Lewis acids) can form various water-stable MOFs.[42] The major classes of water-stable MOFs include the MIL series (MIL-53(Al), MIL-10(Cr), and MIL-53(Fe)), ZIF series, and UIO series. The ZIF series contains Zn^{2+} ions and the imidazolate ligand, which are a soft acid and soft base, respectively.[43] The bond length of the metal–organic coordination bond has an inverse relationship with the stability of the framework. Increasing the bond length reduces the stability due to its impact on the rigidity and dynamic stability of the coordination bond.[38] Moreover, strategies such as enhancing the steric hindrance and providing an additional layer of protection from metal ions effectively prevent water molecules from approaching and attacking the MOF structure.

2.2.2 Hydrophobicity of MOFs. Many of the reported MOFs in the literature were not specifically tested for their hydrophobic characteristics. However, some methods such as water adsorption isotherm measurements, breakthrough experiments involving the competitive adsorption of a vapor mixture containing water and hydrocarbon vapor (typically toluene), and contact angle measurements using liquid water have been reported to analyze the hydrophobicity in MOFs. In certain cases, IR spectroscopy and thermogravimetric analysis have also been utilized to evaluate the hydrophobic properties of MOFs. IR spectroscopy can be employed to qualitatively determine the water content in the hydrophobic pores of MOFs by monitoring the absorption bands near 3600 cm^{-1} for O–H stretching and 1620 cm^{-1} for H–O–H bending of water. Alternatively, TG curves provide information on the amount of water adsorbed by the porous materials and offer insights into the strength of the interactions between the adsorbent and water, as indicated by

the temperature range of weight loss corresponding to adsorbed water molecules.[44]

Internal surface hydrophobization of MOFs is one of the best ways to achieve remarkable stability in water. Hydrophobicity is introduced in the MOF by selecting a suitable ligand or changing the reaction conditions. Guillerm and co-workers[45] compared the synthesis of UIO-66 and MIL-140A based on the reaction between $ZrCl_4$ and $1,4-H_2BDC$ (1,4-benzene dicarboxylic acid) ligand by changing the reaction temperature. The structure of MIL-140A synthesized at elevated temperature was found to be different from that of UiO-66. There were fewer hydrogen-bond acceptor or donor sites on the pore surface of MIL-140A, leading to more hydrophobic character on the MOF surface. Hydrophobic substituents can be incorporated in $1,4-H_2BDC$ ligands to produce a variety of hydrophobic MOFs. A similar MOF was reported by Wu and co-workers by substituting the $H_2BDC-2-CF_3O$ ligand in the MOF skeleton.[46] Another way to introduce hydrophobicity in MOFs to enhance their stability in water is through functionalization with hydrophobic fluorine and/or alkyl/aromatic groups *via* post-synthetic modification techniques (PSM).[47] PSM can be performed to hydrophobize both the internal and external surfaces of MOFs, allowing for a variety of water stabilization techniques.[48] Internal surface hydrophobicity can be achieved through PSM by simple substitution organic reactions under milder conditions such as esterification of the amide or azide group in the ligands.[49]

External surface hydrophobization is another method to enhance the water stability of MOFs, which can could be achieved by modifying their external surfaces with small molecules/ligands, inorganic materials, and organic polymers. One method involves coating MOF crystals with hydrophobic materials. For example, amorphous-carbon-coated MOF-5 exhibited improved stability when soaked in an aqueous solution due to the protective effect of its hydrophobic carbon coating.[50] Meili and co-workers[51] demonstrated a PSM strategy through the one-step radical copolymerization of two monomers, *i.e.*, 2,2,2-tri-fluoroethyl methacrylate (TFEMA) and 3-methacryloxypropyl-trimethoxysilane (MAPTMS), on the surface of HKUST-1. It was reported that this polymeric hydrophobic coating had no effect on the pore characteristics of the original HKUST-1 MOF. Similar external hydrophobicity was introduced in MIL-101 MOF composites through the vapor-phase deposition of poly-dimethylsiloxane (PDMS). Internal hydrophobicity and intact pore characteristics were also reported after successfully introducing PDMS in the composite.[52]

In another study, Liu and co-workers[53] demonstrated the hydrophobization of ZIF-8 through a PSM ligand exchange reaction on the external surface of the crystals. This modification involved replacing the 2-methylimidazolate ligands with a more hydrophobic ligand, *i.e.*, 5,6-dimethylbenzimidazolate (DMBIM), resulting in the formation of ZIF-8-DMBIM. The modified ZIF-8-DMBIM exhibited enhanced hydrophobicity and water stability compared to the original ZIF-8. Various spectroscopic techniques, such as FTIR-ATR, UV-vis, and Raman spectroscopy, together with water contact angle measurements confirmed the successful ligand exchange and demonstrated the improved hydrophobicity of the external surface. Notably,

the BET surface area and pore volume of ZIF-8-DMBIM were only slightly lower than that of ZIF-8, indicating that the ligand exchange occurred primarily on its surface.

In situ external surface hydrophobization of an MOF was also reported by Zu and co-workers.[54] HKUST-1/graphite oxide composites were synthesized with different amounts of graphite oxide in a solution containing the starting materials for HKUST-1. The SEM images revealed that the composites consisted of thin platelets stacked together, which differed from the octahedral-shaped crystals of HKUST-1 and the dense agglomerates of stacked graphene sheets of graphite oxide. The composites showed higher surface areas and pore volumes compared to the pristine HKUST-1. The formation of extra minor meso/macropores in the composites was also reported between HKUST-1 and the graphene layers. After exposure to water vapor at 90 °C, the resultant composite remained structurally unchanged.

Although the hydrophobization of MOFs offers significant advantages for strengthening their water stability and broadening their possible applications, several constraints must be considered. In addition, excessive hydrophobization may result in lower porosity and absorption capacity, thus impacting the overall performance of the material.

2.3 Ionic MOFs for water remediation

The negative charge of the organic ligands often neutralizes the positive charge of the metal ion, making the majority of MOFs electrically neutral. However, sometimes, MOFs possess residual charges in the form of non-framework ions, which makes them ionic MOFs (iMOFs).[55] Due to their distinctive features, these iMOFs have attracted considerable interest in the past few years.[56] In ions in the channels of iMOFs may interact with guest molecules, resulting in tailored interactions with guest molecules in different applications. Based on their charge nature, there are two types of iMOFs, *i.e.*, anionic frameworks, where the framework itself is anionic and requires a counter-cation to maintain its overall charge neutrality, and cationic frameworks, where their cationic nature requires the presence of anions to balance the charge.[57] These polarised MOFs can exchange their ions for external ions, making them promising candidates as ion exchange resins and materials in water purification processes.[58]

The properties of ionic MOFs are affected by the counter ion in their framework.[59] The water stability of iMOFs also depends on the type of counter ion present in their skeleton. For example, larger and more hydrophobic alkylammonium cations have higher water stability than smaller and more hydrophilic cations. These findings imply that the water stability of ionic MOFs can be altered through ion exchange, allowing for the addition of additional hydrophobic ions to improve their stability. It is also feasible to integrate various ions in MOFs, which improves their water stability during application.[60]

The synthetic approaches adopted for the preparation of anionic and cationic MOFs include both pre- and post-synthetic approaches. The *in situ* synthesis of anionic MOFs involves the use of negatively charged secondary building units (SBU).[61]

Zeolite-like MOFs (ZMOFs) are examples of anionic MOFs derived from the reaction between 2-cyanopyrimidine (2-PmCN) and $Cd(NO_3)_2 \cdot 4H_2O$ in DMF and water.[62] A similar ZMOF was also reported by other researchers utilizing 4,5-imidazoledicarboxylic acid (H_3ImDC) as a ligand. The authors reported the similar zeolite-like topology and similar ion exchange capabilities of anionic ZMOF.[63] The construction of cationic MOF involves the utilization of neutral ligands. Among the nitrogen-based ligands, 4-4′-bipyridine (bpy) is the most commonly used ligand for synthesizing cationic MOFs. Hasegawa and co-workers[64] synthesized a 3D cationic MOF structure using the 4-BTAPA (1,3,5-benzene tricarboxylic acid tris[N-(4-pyridyl) amide]) ligand. The directional amide group in ligands acts as a potential candidate for guest interactions in porous structures. The authors also suggested that the choice of the metal salt precursor during the synthesis affects the porosity of the resultant material. The use of nitrate metal salts during the preparation process results in weaker participation of the anions, leading to the formation of a porous cationic framework, whereas chloride metal salts result in stronger interactions of the anions with the amide moieties in the framework, creating a non-porous structure.

One of the most difficult tasks in the field of MOFs is post-synthetically synthesizing an anionic MOF. After the initial synthesis of the parent MOF, this procedure entails changing its structure while maintaining its porosity. To achieve successful post-synthetic alterations, the parent MOF must contain inorganic or organic units with chemical transformation sites. Ameloot and co-workers[65] utilized the most robust and stable UiO-66 ($Zr_6O_4(OH)_4(BDC)_6$) to graft lithium tert-butoxide (LiOtBu) on the framework. The dehydrated UIO-66 precursor contained coordinatively unsaturated Zr^{4+} Lewis acidic sites. Grafting led to the coordination of the tert-butoxide anion to the metal center. This led to the formation of an anionic framework, and consequently lithium ions were trapped in the framework as extra counter anions. Grafting the $tBuO^-$ anion has an important consequence, where it effectively screens the negative charge and facilitates cation mobility.

3. Removal of water contaminants through adsorption

MOFs are growing hot spots in materials science due to their versatile properties.[66] Recently, many reports appeared in the literature on the application of MOFs for the removal of various organic pollutants from water through adsorption.[67–70] The stability of MOFs within a large pH range for a longer experimental period and their reusability compared to other adsorbents make them suitable materials for the adsorption of several water pollutants. The various possible modes of interactions between MOFs and adsorbates are responsible for their high adsorption efficiency (Fig. 2). However, the potential mechanism for the successful removal of contaminants from water follows the order of electrostatic interactions > H-bonding > π–π interactions/stacking > hydrophobic interactions ≈ acid–base interactions ≈ metal effects, etc., which are further

influenced by the chemistry of water and pH of the solution (Fig. 3).[71,72]

3.1 Removal of dyes using MOFs

Among the various pollutants of major concern, dyes contribute to a major portion of water contamination.[73] Organic dyes are extensively used in various industries to impart color to numerous substances and their discharge into the water bodies creates abundant water pollution. Thus, dye removal is an important aspect to consider during wastewater treatment. In this case, various MOFs have been developed for the absorption of different dyes.

3.1.1 Removal of cationic dyes using MOFs. Methylene blue is a cationic dye extensively used in the textile industry. However, due to its toxicity, high color, decreased light penetration in water, high stability, and low degradation potential, the removal of this dye from water is crucial. UiO-66 showed an overall adsorption capacity of 90 mg g^{-1} with 50 mg L^{-1} initial concentration of dye, and hence has great potential to remove methylene blue from aqueous solution.[74] In another study, an MOF based on copper benzene tricarboxylate ($Cu_3(BTC)_2$) was evaluated for the adsorptive removal of basic fuchsin (BF), crystal violet (CV), and Eriochrome Black T (EBT).[75] The findings indicate that the adsorption of BF on the MOF was 99.42% in the post-synthesis process, while 91.47% in the one-step synthesis when BF was incorporated in an organic solution, and 96.54% when BF was incorporated in a metallic solution. In another analysis, a novel copper-based MOF immobilized on graphene oxide (GO) was synthesized via an ultrasonic process as an adsorbent (GO-Cu-MOF) for the adsorptive removal of methylene blue dye.[76] The different studies showed that GO was exfoliated in the Cu-MOF structure, which improved the capacity of GO-Cu-MOF compared to Cu-MOF. Compared to Cu-MOF nanoparticles, GO-Cu-MOF showed a higher surface area, pore size, negative charge, and more active groups, resulting in 20% higher dye removal. Furthermore, GO-Cu-MOF possessed a higher adsorption capacity of 173, 251, and 262 mg g^{-1} at 25 °C, 45 °C, and 65 °C compared to that of 106, 117, and 142 mg g^{-1} for Cu-MOF at the same temperature, respectively. In another work, the water-stable cationic MOF ZJU-48 with one-dimensional pores of around 9.1 × 9.1 Å^2 was synthesized and explored for the adsorption and separation for dyes with different charges and sizes.[77] ZJU-48 displayed excellent water stability for approximately one week, indicating its potential use for adsorption and dye separation. The results showed that the maximum loaded volume of MOF to methylene blue was 582.44 mg g^{-1} and approximately 90% of the loaded dye was released over 6 h from the framework in N,N-dimethylformamide with NaCl, exhibiting adequate adsorptive properties and reusable adsorbent possibilities. As an excellent adsorbent, ZJU-48 can be used not only for cationic dyes but also for small organic molecules.

In another study, CuMOF-1 and CoMOF-2 were synthesized, characterized, and investigated for magnetism and dye adsorption applications.[78] The surprising nature of the structure of CoMOF-2 is that one bpy ligand is coordinated with

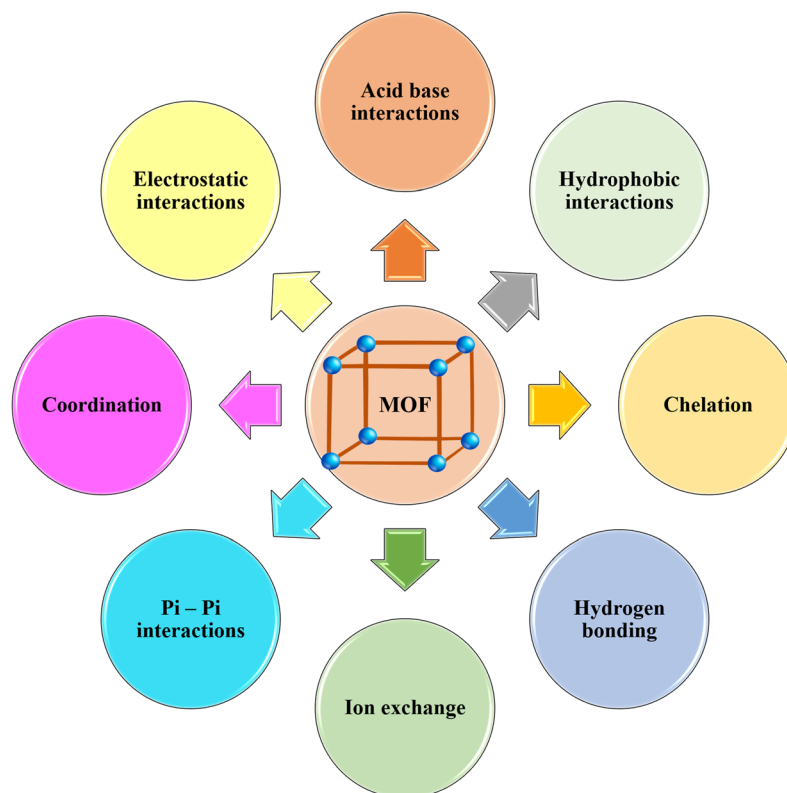# MOF interaction/adsorption mechanism with contaminants (metal ions/ dyes/ pharmaceuticals/ pesticides)

Fig. 3 Various possible mechanisms for the removal of pollutants using MOFs as adsorbents.

cobalt, while one bpy ligand is present between the layers in its lattice, thus consolidating the structure through heavy hydrogen bonding with adjacent units coordinated by water molecules. Furthermore, the adsorption properties of the MOFs against two dyes, i.e., MB and MO, which are organic contaminants, were investigated. The adsorption studies confirmed that the stronger selective adsorbent for MB was CoMOF-2.

Researchers reported the synthesis of two new three-dimensional (3D) anionic Zn-MOFs, i.e., NKU-102 and NKU-103, through solvothermal methods at different temperatures.[79] NKU-102 possessed a sealed 3D structure based on an octahedral cage and showed negligible organic dye adsorption capacity. In contrast, NKU-103 possessed an open triangular microchannel surrounded by two types of helical chains, and therefore exhibited excellent size-selective adsorption towards small organic cationic dyes.

Copper–benzene-tricarboxylate-based MOFs, Cu-BTC, with a mesoporous structure, high surface area and wide pore volume have been used for the adsorption of MB.[80] Lin et al. investigated the potential mechanism and adsorption of MB by Cu-BTC. After washing with ethanol, the Cu-BTC adsorbent could easily be regenerated. The experimental results showed that the Cu-BTC materials adsorbed MB dye, and thus have potential applications for wastewater treatment. An enthalpy modification rather than an entropy effect was the driving force of MB adsorption on Cu-BTC.

A quick, swift mechanochemical method using a kitchen grinder was used to develop MOFs. By implementing this instrument, researchers synthesized multi-gram-scale ZIF-8, CuBTC, and MIL-100IJFe and successfully used MIL-100IJFe-KG for the effective removal of MB dye from an aqueous solution. This study explored new aspects for the simple, convenient, and green synthesis of MOF materials using a common technique, and their use in wastewater treatment was investigated.[81]

In another study,[82] a novel nanohybrid, MIL101-Cr/PANI/Ag, based on a Cr-MOF was designed and developed by a hydrothermal method and characterized using various sophisticated analytical techniques as an adsorbent for MB dye. The adsorption studies were carried out by varying different parameters including mass, initial dye concentration, pH, and temperature. The maximum adsorption efficiency observed for MB dye using the synthesized MOFs was 43.29 mg g^{-1} with the mechanism of H-bonding between the amine groups of PANI/Ag with the nitrogen present in the MB structure and the surface hydroxyl groups of MIL101-with MB molecules. In addition, π–π stacking interactions were observed between the aromatic rings of the dye molecules and MIL101-Cr and PANI in MIL101-Cr/PANI/Ag structure. The adsorbent was found to be effective and stable for up to four consecutive cycles. ZIF-8 was created by crosslinking carboxymethyl cellulose to the surface of a nonwoven fibrous polyester sponge, which was then utilized to remove MB

dye from an aqueous solution. At concentrations of 2, 5, and 8 mg L^{-1}, the MOF adsorption capacity was 0.083, 0.466, and 0.824 mg g^{-1} in a continuous system and 0.160, 0.568, and 0.829 mg g^{-1} in a batch system, respectively. Its adsorption capacity was improved by roughly 80% and 90% in the batch and continuous systems, respectively, when the starting dye concentration was increased from 2 to 8 mg L^{-1}.[83] In another report,[84] a TiO$_2$@Cu-MOF nanocomposite was synthesized using copper nitrate trihydrate as the copper source and the effect of the TiO$_2$ loading on the adsorption of rhodamine B was investigated. The outcomes demonstrated that the composite material not only exhibited good rhodamine B degradability (98.03% of the dye was removed after 120 min) but also exhibited a good cycle performance. By using the cationic surfactant cetyltrimethylammonium bromide (CTAB) as a supramolecular template, the hierarchically mesostructured MIL-101 was successfully synthesized under solvothermal conditions.[85] In the preparation of MIL-101 nanoparticles, the surfactant CTAB was found to play an important role. Significantly, in comparison to the bulk MIL-101 crystals, the hierarchically mesostructured MIL-101 exhibited remarkably accelerated adsorption kinetics for MB dye removal due to the presence of unique hierarchically meso- and macropores in the solid. In another study, a rapid and ecofriendly sonication method was used for the synthesis and immobilization of Ag-MOF and Cu-MOF on or between graphene oxide (GO) sheets. GO-Ag-MOF and GO-Cu-MOF displayed improved physicochemical properties, including enhanced surface area, surface charge, and active adsorption sites with the aid of characterization methods such as zeta potential, Brunauer–Emmett–Teller (BET), X-ray diffraction (XRD), and scanning electron microscopy.[86] Both GO-Ag-MOF and the GO-Cu-MOF showed an approximately 10% increase in adsorption capacity for MB dye in comparison to the pristine Ag-MOF and Cu-MOF under all the tested conditions, respectively. More than 98% of the MB dye was removed by GO-Ag-MOF, followed by Ag-MOF (90%), GO-Cu-MOF (75%), and Cu- MOF (65%). In another report, MIL-101 was loaded with zinc tetraphenylporphyrin (ZnTPP) to form Zn[TPP]@MIL-101 for adsorptive and photocatalytic MB dye removal.[87]

3.1.2 Removal of anionic dyes using MOFs. García et al. reported the development of the [Fe(BTC)] MOF for the adsorptive removal of azo-dye Orange II from aqueous solutions.[88] The adsorption potential of [Fe(BTC)] was reported to be five-times higher than that of activated carbon. The removal was influenced by the operational parameters, such as adsorbent mass, temperature, contact time, and initial dye concentration. The maximum monolayer adsorption capacity of Fe(BTC) was 435 mg g^{-1} at 298 K, which was reported to decrease with an increase in temperature. Zhang et al.[89] reported new ZIFs as adsorbents with high chemical and thermal stability for the adsorptive removal of azo dyes. The experimental data indicated that the main driving force for the high adsorption was the electrostatic attraction between ZIF-67 and Congo red together with π–π stacking.

MIL-68(Al) was synthesized and its adsorption activity investigate using methyl orange (MO).[90] Its adsorption isotherm was confirmed to follow the Langmuir isotherm model and its maximum equilibrium adsorption was determined to be 341.30 mg g^{-1}. The thermodynamic data showed that the method of adsorption was spontaneous and endothermic. In addition, after the adsorption of MO, MIL-68(Al) retained its original structure. This study expanded the scope and potential applications of MIL-68(Al) as a new adsorbent for the removal of MO from wastewater.

A cationic Cd-MOF with a 1-D channel effective pore volume of 53% was synthesized and found to exhibit a wide adsorption rate, where anionic dye molecules can be adsorbed effectively, while neutral and cationic dye molecules cannot be adsorbed according to its color changes.[91] In the presence of NaCl, anionic dye molecules were observed to be slowly released, suggesting that this material may be a possible anionic adsorbent that remains stable for up to six consecutive cycles. In one study, polymorphic MOFs, ZIF-8, ZIF-L, and dia(Zn), were evaluated for their dye sorption performance. These three polymorphs possess identical metal ions, i.e., Zn(II) ions, and organic ligands (2-methylimidazole); however, they differ in terms of crystal structure and crystal morphology.[92] For the formation of ZIF-L membranes on a porous alumina substrate, researchers developed a wet deposition method using stabilized ZIF-L suspensions. It was observed that ZIF-L showed the highest sorption potential for Rose Bengal dye molecules, which possessed free molecules of imidazole that leached in the water during sorption. Up to 95% of the dye solution was extracted using the synthesized ZIF-L adsorbent under the optimum conditions.

Utilizing the solvothermal reaction of cobalt(II) salts and HTBC as a triangular linker, two porous MOFs, {[Co$_{0.5}$(TBC)]·2DMF}$_n$ (1) and {[Co(TBC)-Cl$_{0.5}$(CH$_3$OH)]·0.5Cl}$_n$ (2), were synthesized.[93] In an aqueous solution, compound 2 exhibited selective adsorption properties for the anionic MO. The dye adsorption studies with 1 and 2 showed that two significant factors significantly affected the dye adsorption, i.e., the porous character and charge properties of the MOFs. Thus, 1 was shown to be highly useful for dye-related environmental contamination applications because of its excellent selective adsorption and desorption properties, as well as its easy preparation and convenient handling. It was reported that the incorporation of Ag nanoparticles in UiO-66 MOF enhanced the adsorption of indigo carmine (IC) dye from 87.2 mg g^{-1} to 312 mg g^{-1} at 2 wt% Ag/UiO66.[94] This enhancement in adsorption capacity was attributed to the enhancement of the number of adsorption sites and pi–pi interaction between IC and Ag-UiO-66.

With or without further functionalization, the adsorptive removal of four dyes with nitro or sulfonate groups was carried out using highly porous MIL101s.[95] Among them, melamine-functionalized MIL101 (MIL101-Mela) was successful in removing Martius yellow (MY), naphthol yellow S, orange G, and sunset yellow FCF. According to the adsorption data, the dye removal efficacy increased by increasing the amount of hydrogen donors and acceptors in the adsorbents and dyes, respectively. The adsorbents and dyes act as hydrogen donors and acceptors in hydrogen bonding, which is proposed as the

primary mechanism of adsorption. With more hydrogen bonding sites producing six-membered rings, the adsorption of dyes can be quantitatively improved. Activated carbon (AC) is an inert adsorbent substance that has been commonly used for the treatment of water or the recovery of water from environmental pollutants. Researchers prepared AC@MIL-101(Cr) as a highly porous adsorbent composite.[96] Under near-neutral pH conditions, the kinetics of the AC@MIL-101(Cr) composite for organic dye removal was faster than MIL-101(Cr) for anionic dyes (direct red 31 and acid blue 92). This study offers a new concept for the design and synthesis of highly efficient MOF-based nanoporous adsorbents for the removal of pollutants and organic dyes from wastewater.

3.1.3 Removal of cationic and anionic dyes using MOFs. Hassan *et al.*[97] reported the removal of two pollutants, *i.e.*, anionic and cationic dyes, from wastewater using MIL-101[Fe] through adsorption processes. Compared to AC adsorption, the adsorption potential of MO and MB dyes on MIL-101[Fe] was extremely high.

In another study,[98] the potential of nickel-dependent MOFs (1,3-bis(4-carboxyphenylimidazolium)chloride and 1,3-bis(3,5-dicarboxyphenylimidazolium)chloride) for the adsorption of charged and neutral dye molecules was evaluated. The adsorption and analysis data showed 81.08% and 98.65% removal efficiency of MO and CR, respectively, which indicated their potential for the successful adsorptive removal of positively charged dyes.

Li *et al.*[99] reported the synthesis of a new MOF, HU21, *via* a hydrothermal reaction, which showed a high photocatalytic rate for the removal of MB dye, although the adsorption quantity of MB and MO dye was almost the same. The degradation of MB dye reached 248 mg g^{-1} under light irritation and the photocatalytic activity reached 96.1%.

In another study, three different MOFs, UiO-66, UiO-67, and MIL-100[Fe], were used as adsorbents for four dye molecules (MB, rhodamine B, tropaeolin O, and amaranth).[100] The results indicated that the surface properties and matrix structure of the MOFs influenced their dye adsorption ability and kinetics. UiO-67 has a charge-neutral framework structure with a uniform pore size, enabling the adsorption of both positively and negatively charged dyes. For various forms of dyes, MIL-100[Fe] displayed similar adsorption trends to UiO-67. However, MIL-100[Fe] exhibited lower dye adsorption than UiO-67 because of its smaller surface area. More significantly, the dye adsorption properties of the MOFs could be significantly influenced by their tunable surface functionality based on defect site regulation.[100]

Two isostructural MOFs, namely, Co-MOF and Ni-MOF, were reported for the adsorption of five different dye molecules (CR, MO, MB, methyl blue, and rhodamine B (RhB)).[101] The results showed that Co-MOF efficiently absorbed CR due to the hydrogen bonding and π–π stacking interactions between them. The electrochemical efficiency tests showed that compared to Ni-MOF, Co-MOF exhibited a better rate capability. Because of its peroxidase-like behavior, MOF-545[Fe] was synthesized to extract dyes.[102] The adsorption behavior of MOF-545[Fe] for the acidic (anionic) dye MO was higher than that for the basic (cationic) MB dye. This adsorbent resulted in significant color fading over a short period (about 2 h) for MO and MB due to its peroxidase-like activity.

Recently, the synthesis of two types of bimetallic cationic MOFs named PFC-24-Zr and PFC-24-Hf with the integration of backbone charges *via* the solvothermal method was reported.[103] This combination not only created robust coordination bonds during the self-assembly process but also left net charges on the metal clusters, providing a method for the rational design of bimetallic cationic MOFs. PFC-24-Zr showed obvious absorption of MO (anionic dye) with little absorption for MB (cationic dye) and methyl yellow (MY, neutral dye) although these three dyes have similar molecular sizes, and it could also be applied for the efficient removal of $Cr_2O_7^{2-}$.

The synthesis and characterization of Ce(III)-doped nanocrystals of UiO-66 were reported, which showed their ability to effectively extract organic dyes from aqueous solutions.[104] Doping with Ce(III) increased the number of adsorption sites and induced π–π interactions between the adsorbent and adsorbate, thus increasing the ability to adsorb cationic and anionic dyes and overcoming the effect of electrostatic interactions.

Recently, the application of UiO-66-NH$_2$@poly sodium 4-styrene sulphonate (UiO-66-NH$_2$@polyNass) was reported for the high and selective adsorption of various acidic, neutral, and basic dye molecules. In this study, UiO-66-NH$_2$ functioned as a substrate, where amino groups existed as a covalent anchoring point for the installation of α-bromoisobutyryl bromide (BiBB), and poly(Nass) brushes were grafted on the surface to obtain the UiO-66-NH$_2$@poly(Nass) composite. The highest adsorption capacity was observed for basic MB dye (299.8 mg g^{-1}) and basic fuchsine (789.2 mg g^{-1}) on UiO-66-NH$_2$@polyNass compared to neutral dyes (Sudan and neutral red) and acidic dyes (acid orange and acid chrome blue k) due to the multiple interactions between the dye molecules and UiO-66-NH$_2$@polyNass with sulfonic groups and amino groups, conjugation between the benzene rings of the adsorbents and aromatic dyes, and hydrogen bonding provided by the sulfonic, amino and carboxyl groups in UiO-66-NH$_2$@polyNass with the dyes.

Another report[105] described the synthesis of magnetic porous carbon using a two-step, straightforward process from a mixed MOF. A magnetic precursor called MOF-74(Zn/Fe) produced at ambient temperature was used to create very porous magnetic carbons. The adsorption isotherms of MB and MO were recorded and compared with that produced using a non-magnetic MOF-74(Zn)-derived porous carbon to evaluate the potential of the magnetic MOF-74(Zn/Fe)-derived porous carbon as a sorbent. It exhibited higher maximum adsorption capacities for MB and MO dyes than the other magnetic adsorbents at 370 and 239 mg g^{-1}, respectively. The zeta potential studies and other investigations showed that dye extraction at various pH levels occurred by electrostatic interactions, which play a significant role in dye removal.

In a recent investigation,[106] CoMOF (KIUB-OF-1) was selected as a representative to adsorb cationic and anionic dyes such as MO, MB, and malachite green (MG) from brackish water, which was successfully synthesized *via* straightforward stirring in

water as the solvent. CoMOF exhibited exceptional adsorption capacities of 15 610, 14 721, and 5083 mg g^{-1} for MO, MB, and MG, respectively, at 35 °C, indicating that it is an effective adsorbent for these pollutants. Furthermore, this MOF exhibited the advantages of being regenerated and stability, which showed up to 90% removal even after four cycles.

Hexahedral NH$_2$-MIL88[Fe] with an enormous surface area (865.59 m^2 g^{-1}) was prepared using the solvothermal method and explored for the adsorption of MB and acid red 57 (AR57). Temperature, contact time, and pH all had a significant impact on the dye adsorption, where the maximum adsorption of 591.72 and 1014 mg g^{-1} for MB and AR57 was attained at pH 9 and 3, respectively. The adsorption was endothermic because the movement of the molecules resulted in an increase in temperature, increasing the efficiency of dye elimination, which caused the free Gibbs energy of both dyes to be negative. Thus, it was proposed that the synthetic NH$_2$-MIL88[Fe] is a promising material for the removal of dyes.[107]

3.2 Removal of metal ions using MOFs

Heavy metal ions are the most common water pollutants caused by various industrial activities, creating a major environmental problem. Their high concentration and degradation is an environmental concern, which need to be dealt with urgently. Detailed reviews summarizing the removal of metals by various processes and techniques are available in the literature.[70,108] In recent years, MOFs have been demonstrated to be potent candidates for metal removal, as documented in the literature.[109–111] The Zr-MOF characterized with uniform pore size, high porosity, and specific functional groups showed enhanced adsorption capacities for the efficient removal of toxic metal ions from aqueous media.[112]

3.2.1 Removal of lead ions by MOFs.
Recently, Arjmand et al. reported the removal of heavy metal ions using ethylene diamine-functionalized UiO-66-EDA (synthesized by Michael addition reaction).[113] Under the optimized experimental conditions, the maximum adsorption capacity (with an initial metal ion concentration of 300 mg L^{-1}) for Pb(II), Cd(II), and Cu(II) ions was reported to be 244, 217.3, and 208.33 mg g^{-1}, respectively. Monolayer chemisorption was the suggested adsorption phenomenon, as shown by the Langmuir adsorption data, and followed pseudo-second-order kinetics. Electron exchange, electron sharing, and electrostatic and covalent interactions between the metal ions and UiO-66-EDA functional groups were the main mechanisms involved during the adsorption phenomenon. The highest adsorption capacity of Pb(II) ions was attributed to its high electronegativity compared to Cu and Cd ions, which could form a stable complex with a lone pair of electrons on the nitrogen of the amine group. Fig. 4 shows the effect of pH on the adsorption mechanism. The removal capacity for Pb(II), Cd(II), and Cu(II) ions was reported to be 84%, 76%, and 67%, respectively, after four consecutive adsorption–desorption cycles.

To overcome the instability of MOFs, the hydrothermal method was utilized for the development of composites, where the sandwiched-structured MIL-101[Fe] was modified with graphene oxide (GO).[114] The insertion of GO in the MOF led to an increase in the number of active sites and a decrease in surface area, with the maximum adsorption capacity of 128.6 mg g^{-1} for Pb(II) ions at pH 6. The adsorption mechanism was governed by ion exchange with four consecutive regeneration cycles, as characterized by the monolayer chemisorption adsorption isotherm.

In a recent study,[115] researchers reported the synthesis of UiO-66-NH$_2$ via the microwave heating method, which was incorporated in electrospun polyacrylonitrile (PAN)/chitosan nanofibrous membranes (Fig. 5). The developed nanofibrous material was further explored for the removal of Pb(II), Cd(II), and Cr(VI) ions via the adsorption and membrane filtration processes. The synthesized material was characterized by various sophisticated analytical techniques, which indicated the homogeneous distribution of MOF crystals on the nanofiber surface of up to 10 wt% UiO-66-NH$_2$ with a surface area of 1118 m^2 g^{-1}. As an adsorbent, the developed nanofibrous material showed the maximum adsorption capacity of 441.2, 415.6, and 372.6 mg g^{-1} for Pb(II), Cd(II), and Cr(VI), respectively. The researchers claimed that the PAN/chitosan/UiO-66-NH$_2$ nanofibrous adsorbent with a large specific area and functional groups such as carboxylic, amine, hydroxyl, and oxygen for chelating with metal ions resulted in a higher sorption efficiency compared with other studied adsorbents. The adsorption data were found to follow the Redlich-Peterson isotherm for five consecutive regeneration cycles.

A study on the hydrothermal synthesis and structural characterization of a new 3D MOF-1 was reported.[116] Under mild conditions at around pH 6, MOF-1 and its nanostructure were used to adsorb heavy metal ions including Pb(II), Hg(II), Cd(II), Al(III), and Fe(III). The findings revealed that MOF-1 can act as an effective sorbent for the removal of these metal ions, while remaining structurally stable throughout the process.

The efficient adsorptive removal of Pb(II) from aqueous media was demonstrated by mesoporous MOF-5 with the composition of Zn$_4$O(BDC)$_3$, to form a 3-D structure.[117] At pH 5 and 45 °C, the adsorption of Pb(II) ions on MOF-5 formed a monolayer with a high adsorptive capacity (658.5 mg g^{-1}) according to the Langmuir model. Furthermore, changing the pH of the aqueous solution increased the adsorptive removal
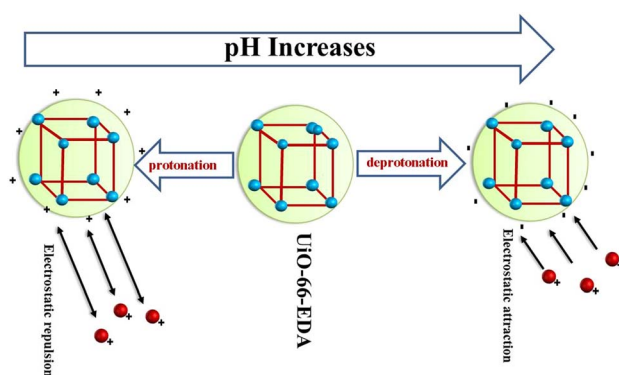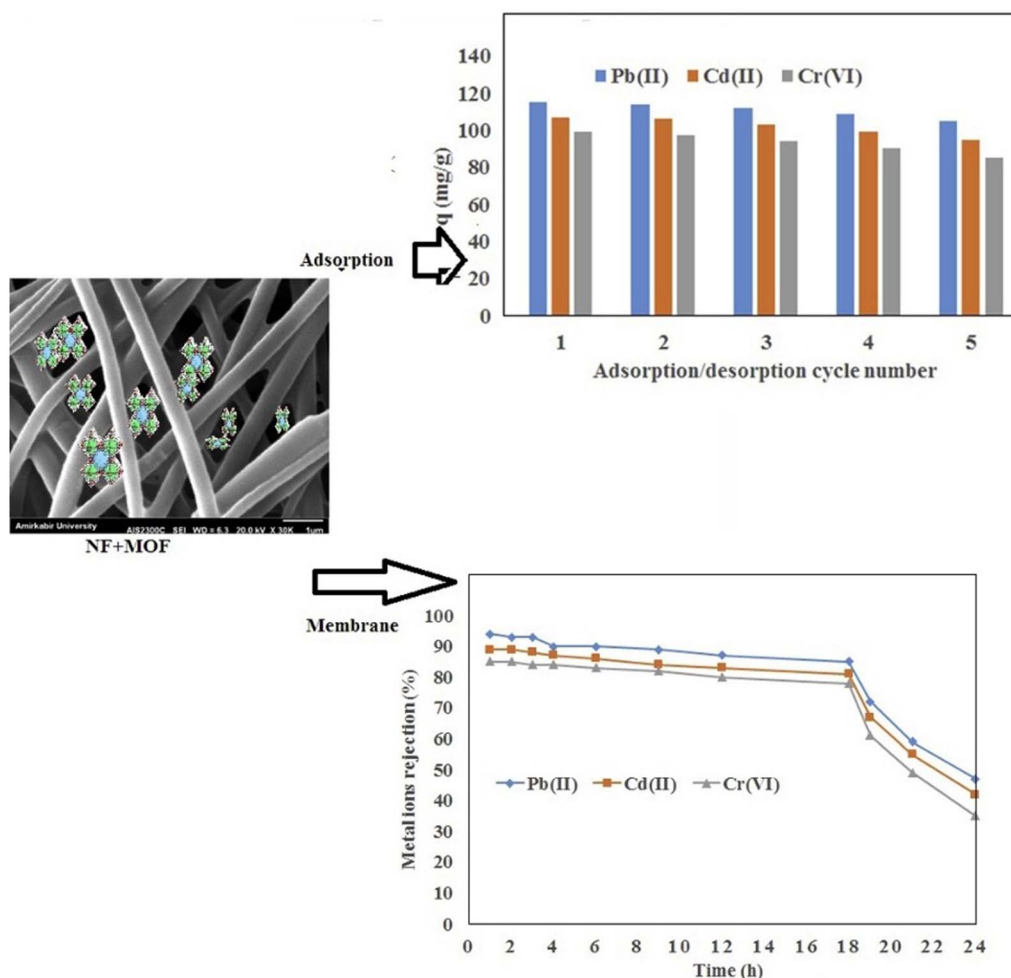

Fig. 4 Effect of pH on adsorption.

Fig. 5 Application of nanofibers/MOFs in the removal of metal ions (reproduced with permission from ref. 115).

capacity of Pb(II) ions. Despite the loss of structural stability caused by the presence of water, it was concluded that MOF-5 is a very effective adsorbent material for the removal of Pb(II) ions from wastewater.

The organic linker terephthalic acid was used to make a nickel(II)-based (MOF).[118] This MOF was characterized and used as an adsorbent to remove lead ions from aqueous solutions. The maximum adsorption occurred in an acidic medium according to this study, which was detected after 45 min of contact time.

3.2.2 Removal of cadmium ions using MOFs. The water-stable Zr-based MOF-808 was supported on PAN nanofibers synthesized through co-electrospinning in electrospun nanofiber composite membranes.[119] The sequestration Cd^{2+} and Zn^{2+} ions was used to determine the membrane performance in batch filtration for heavy metal ion adsorption. The adsorption capacities of the pristine MOF and MOF composite membranes showed that the MOF particles in the membrane could be accessed for adsorption in the hydrophilic PAN membranes. The high separation performance and reusability of the developed membrane, as well as the excellent water stability of the MOF indicated that it can be used to treat water. The synthesis of the FJI-H9 MOF by reacting $CaCl_2$ with 2,5-

thiophene dicarboxylate was reported, which exhibited high adsorption and selectivity for the reversible uptake of Cd(II) ions.[120] According to this study, the high absorption was due to the extraordinary synergy between the active sites and the confined cavity. The fast detection of Cd(II) ions at low concentrations of less than 10 ppm and the *in situ* reconstruction of the used framework into a new one were observed. All these characteristics of FJI-H9, including high adsorption, regeneration, and detection speed, provide a new approach for developing more efficient adsorbents to remove and detect heavy metal ions (Fig. 6).

The removal of cadmium ions from an aqueous solution was investigated using a Cu-MOF.[121] The amount of Cd(II) adsorbed on the Cu-MOF adsorbent increased with an increase in the contact time, initial concentration, and adsorbent dosage. The data well-fitted the Langmuir isotherm and the monolayer adsorption capacity of the Cu-MOF was determined to be 219.05 mg g^{-1}. For all the initial Cd(II) ion concentrations, the kinetic studies showed that the pseudo-second-order model had high correlation coefficients.

In a study, a simple and novel approach for designing MOFs with tunable conductivity was developed.[122] Because of the selective and rapid sorption of Cd(II) ions, the *in situ* amine-

functionalized TMU-60 has potential to transform into a conductor. The presence of cadmium ions improved the ability of electrons to transfer between the constituents in the framework (Fig. 7). The achieved tunable and highly stable electrical conductivity was provided by the sorption of metal ions, although the porosity in the structure remained to some extent. The charge transport through the pellet is thought to be based on the hopping between metal nodes and localized Cd(II) after sorption, as evidenced by chronoamperometry measurements. This novel approach not only improves the conductivity of MOFs but also allows their conductivity to be adjusted according to the desired applications.

3.2.3 Removal of radioactive metals using MOFs. The removal of U(VI) and Th(IV) metal ions from an aqueous environment was achieved using a magnetic MOF, *i.e.*, Fe_3O_4@-AMCA-MIL53(Al).[123] This MOF nanocomposite was synthesized by a modified solvothermal method and characterized by TGA, FTIR, SEM-EDX, XRD, HRTEM, BET, VSM (vibrating sample magnetometry), and XPS, followed by batch studies for the removal of radioactive metal ions. The results showed that Fe_3O_4@AMCA-MIL53(Al) was an effective material for removing these radioactive metal ions from aqueous solution (Fig. 8). The maximum adsorption capacity within equilibrium time of 90 min for U(VI) and Th(IV) on the Fe_3O_4@AMCA-MIL53(Al) nanocomposite was 227.3 and 285.7 mg g^{-1}, respectively, *via* the Langmuir model and spontaneous and endothermic, according to the thermodynamic experiments.

In another report, an MOF material was functionalized by grafting the amino group of tetraethylenepentamine (TEPA) to its coordinative unsaturated Cr(III) centers.[124] Among three different quantities of TEPA, the mass ratio of 60 wt% adsorbent of MIL-101-TEPA shows the highest adsorption property, with the maximum adsorption capacity of 350 mg g^{-1} for uranium(VI) from water at pH 4.5. Grafting amines with the proper mass ratio of TEPA on the open metal sites of MOFs was an efficient method of obtaining high adsorption properties for U(VI), and

MIL-101-TEPA 60% was investigated as a promising material for improving U(VI) adsorption from wastewater.

The capture of radioactive iodine safely and efficiently is crucial. CuBi-CO_3-layered double hydroxides (CuBi-CO_3-LDHs) were used as a standardized base and 3D hierarchical flower-like ZIF-67/CuBi-CO_3-LDH composites were built on top of it.[125] The efficient adsorption behavior for iodine was achieved by the presence of special structures and functional groups in the ZIF-67/CuBi-CO_3-LDH composites. The effects of the special layer structure and strong charge transfer between nitrogen imidazole rings and iodine may explain the high adsorption potential for iodine. Thus, the as-prepared ZIF-67/CuBi-CO_3-LDH composites can be considered promising adsorbents for removing iodine.

3.2.4 Removal of chromium ion using MOFs. For the first time, *in situ*, intergrown ZIF-67-based "pearl-necklace-like" composite membranes were prepared on the surface of 2-methylimidazole/cellulose acetate (MIM/CA) electrospun nanofibers.[126] The incubation time was found to have a significant influence on the growth of the ZIF-67 nanoparticles. The ZIF/CA-24 composite membrane had a high adsorption efficiency of 18.9 and 14.5 mg g^{-1} toward Cu(II) and Cr(VI), respectively, with approximate saturation. The prepared MOF composite materials are expected to be promising for removing heavy metal ions from water due to their high removal efficiency, ease of operation, and highly porous structure. A modified Stöber method was used to synthesized thiol-functionalized and amino-functionalized materials based on Cu-BTC MOFs.[127] Under acidic conditions, both functionalized materials demonstrated good adsorption for Cr(VI) ions with an adsorption capacity of 15.17 mg g^{-1} and 7.17 mg g^{-1}, respectively, for up to five adsorption cycles. The functionalized material did not swell during the adsorption process and was insoluble in water. The results showed that these two functionalized MOFs have promising applications in the adsorption and removal of the Cr(VI) heavy metal in an aqueous solution.

3.2.5 Removal of miscellaneous metal ions using MOFs. For the adsorption of some heavy metal ions (Co^{2+}, Cd^{2+}, Cu^{2+}, Cr^{2+}, Fe^{2+}, and Pb^{2+}), researchers have investigated the adsorption behavior of four reticular 3D porous zinc(II) MOFs with the pcu topology, including (TMU-6), (TMU-21), (TMU-23) and (TMU-24), which were successfully synthesized *via* the mechanochemical method.[128] Four isoreticular zinc(II)-based MOFs were chosen with the only difference in the type of functional group (imine or amide) and whether their pillar structure contained phenyl or naphthyl groups. It was discovered that the presence of amide and phenyl groups in the pillars resulted in a higher propensity for metal ion adsorption than the MOFs with imine and naphthyl groups. The various adsorption patterns of the MOFs towards the considered heavy metal ions were due to the electronic structure of the ligands. Finally, TMU-23, with its suitable functional groups, high porosity, and good water stability, as well as its high adsorption efficiency, may be a promising material for use in the extraction and removal of metal ions from water samples, particularly Pb^{2+} ions.
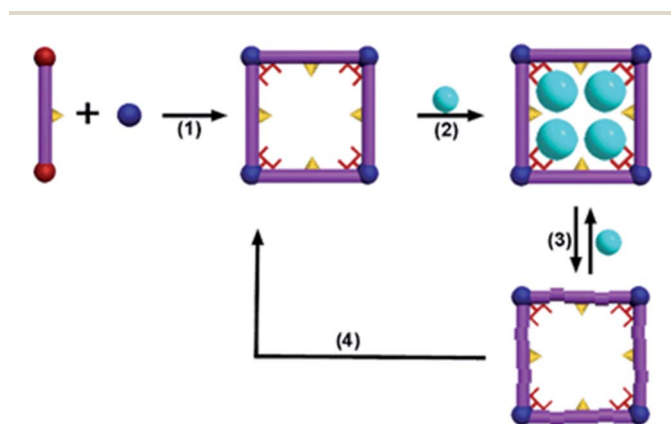

Fig. 6 Regenerative MOFs for the reversible uptake of Cd(II): (1) self-assembly of the 3D framework from the organic ligand and hard metal ion; (2) effective absorption with high capacity; (3) absorption and desorption; (4) reconstruction of the used sample into a fresh sample (reproduced with permission from The Royal Society of Chemistry from ref. 120).
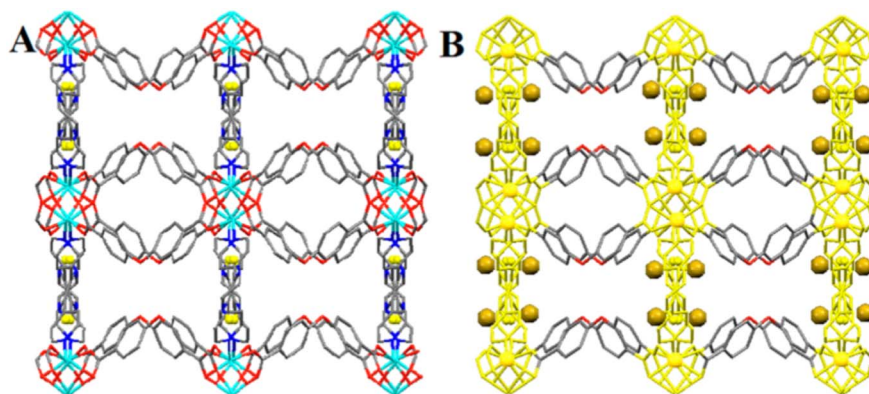
Fig. 7 (A) Schematic representation of TMU-60. (B) Possible pathway for electron transfer in conducting TMU-60-Cd [the golden balls display Cd(II)] (reproduced with permission from ref. 122).

The incorporation of ethylenediaminetetraacetic acid (EDTA) in a strong MOF to create a broad-spectrum heavy metal ion trap was assessed by researchers.[129] The trap was very successful, with removal efficiencies of >99% for single-component adsorption, multi-component adsorption, and breakthrough procedures for a total of 22 heavy metal ions, including hard, soft, and borderline Lewis metal ions. To prepare well-dispersed single or multiple metal catalysts, this material can also be used as a host for metal ion loading with arbitrary amounts/types of metal ions and a controllable uptake ratio. This report proposed a flexible heavy metal ion trap that can be used in separation and catalysis applications.
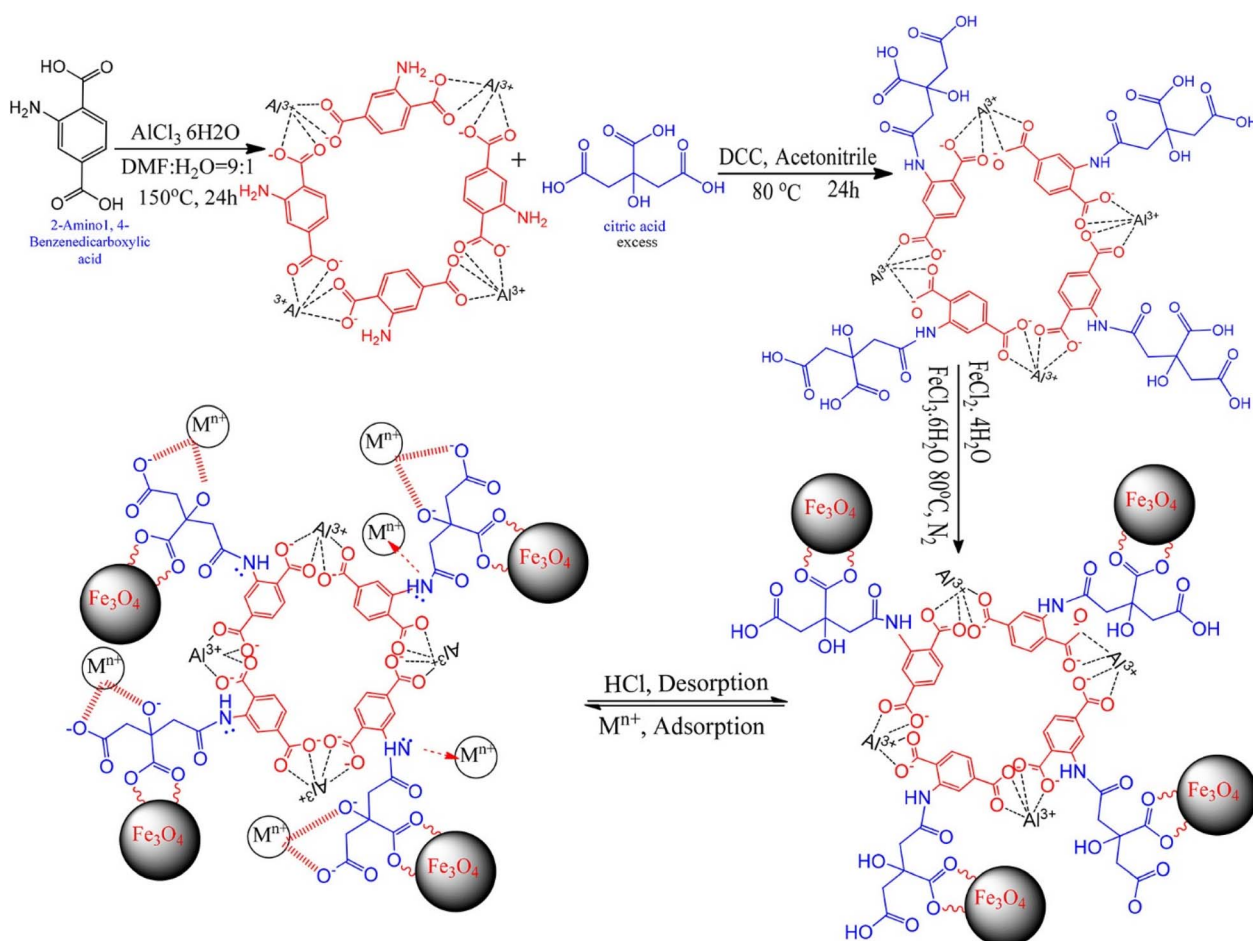

Fig. 8 Synthesis of Fe_3O_4@AMCA-MIL53(Al) nanocomposite and its adsorption–desorption behavior for metal ions (reproduced with permission from ref. 123).

In another study,[130] the HKUST-1 MOF has been synthesized, characterized, and explored for the adsorption of Ce(III) ions from aqueous media. The maximum adsorption capacity was found to be 353 mg g^{-1} at pH 6, following the by Langmuir adsorption isotherm and pseudo-second-order kinetic behavior. The adsorption mechanism was mainly attributed to ion exchange and covalent bonding. However, complete regeneration of the adsorbent using methanol was not achieved.

3.2.6 Removal of heavy metal oxyanions using cationic MOFs.

Ionic MOFs especially cationic MOFs have wide applications as anion receptors and ion exchange materials for the removal of heavy metal ions. Recently, a group of researchers reported the removal of oxyanions using water-stable cationic MOFs (Fig. 9). Firstly, they reported a solvothermal method for the synthesis of water-stable 3D, cationic MOFs(1-SO$_4$) using a tripodal neutral ligand with free sulfate ions for $Cr_2O_7^{2-}$ and MnO_4^{-} ions, with the latter acting as a model for the radioactive contaminant pertechnetate (TcO_4^{-}).[131] Here, a unique MOF with free and ligated sulfate ions was reported. The adsorption of dichromate and manganate ions from aqueous media on MOF-1 was monitored by PXRD, FTIR, and time-dependent UV-vis spectrometry with a visual color change in the metal ion solution. The observed results confirmed the hypothesis that a tetrahedral substitutable anion acts as a facilitator for the capture of toxic-metal oxoanions. Ghosh et al. reported the removal of oxo-anions from water using different ionic MOFs, which were water stable.[132]

To overcome the stability issues of earlier reported cationic MOFs, researchers synthesized a modified version of MOF iMOF-2C with an inbuilt hydrophobic cavity used for the recognition and selection of heavy metal oxyanions for anion exchange via hydrogen bonding.[133] These cationic MOFs showed the highest uptake efficiency for CrO_4^{2-} (476.3 mg g^{-1}) and ReO_4^{-} (691 mg g^{-1}) with reusability for up to 10 cycles. EDX analysis together with other analytical techniques confirmed the anion exchange process with the sulfate ions in the MOFs. In another study, the selective and efficient removal of Se(VI)/As(V)/Se(IV) oxyanions at a very low 1000 ppb level was reported using a chemically stable cationic MOF (iMOF-3C).[134] The maximum adsorption capacities for Se(IV), Se(VI), and As(V) oxyanions on iMOF-3C were reported to be 140 mg g^{-1}, 72 mg g^{-1}, and 75 mg g^{-1}, respectively, and the highest in the literature with monolayer adsorption confirmed via the Langmuir adsorption isotherm (Fig. 10). A real water sample from the Mutha river with 1 ppm of Se(VI)/Se(IV)/As(V) was explored for the removal of the reported oxyanions using iMOF-3C. The results indicated that the oxyanion concentration of Se and As decreased by up to 10 ppb within 24 h, thus suggesting the potential of iMOF-3C as a cationic adsorbent in the presence of other competitive ions. Table 1 presents a summary of the application of MOFs in the removal of common metal ions through adsorption.
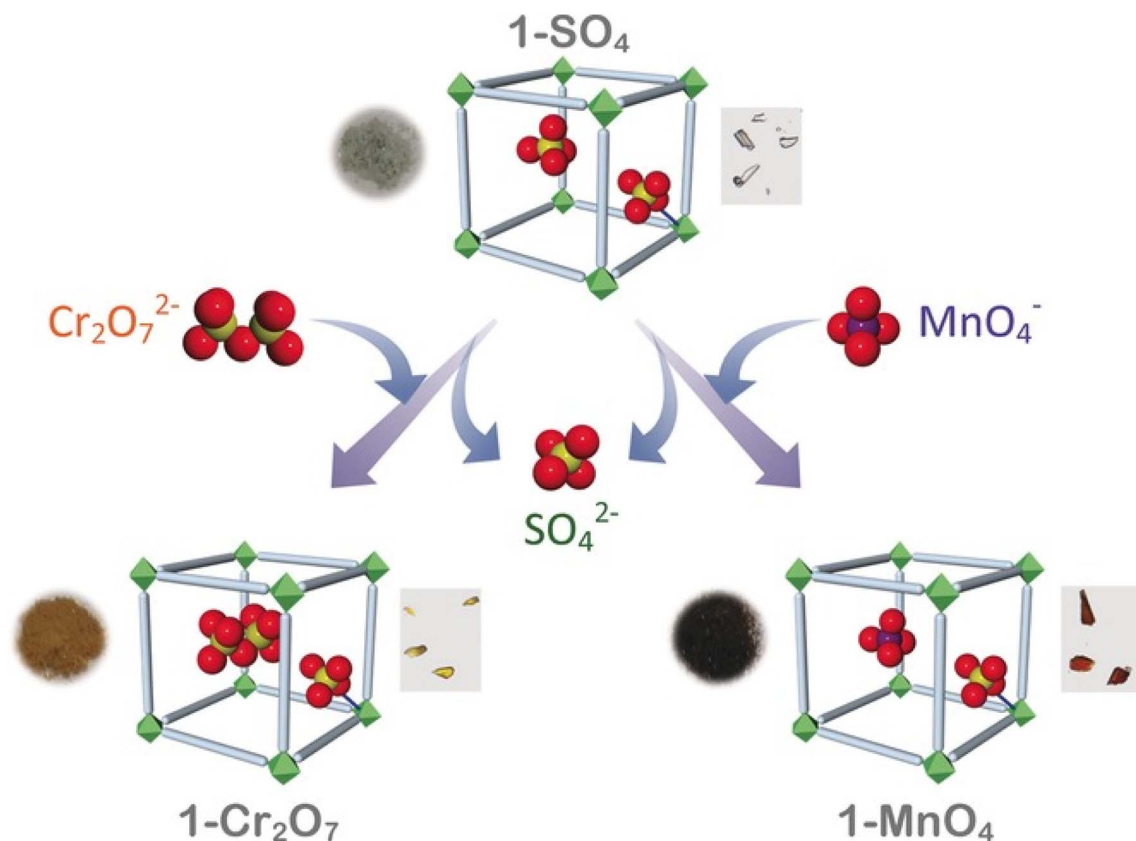

Fig. 9 Schematic representation of the capture of heavy metal oxoanions by 1-SO$_4$ with concurrent loss of SO_4^{2-} (reproduced with permission from ref. 131).
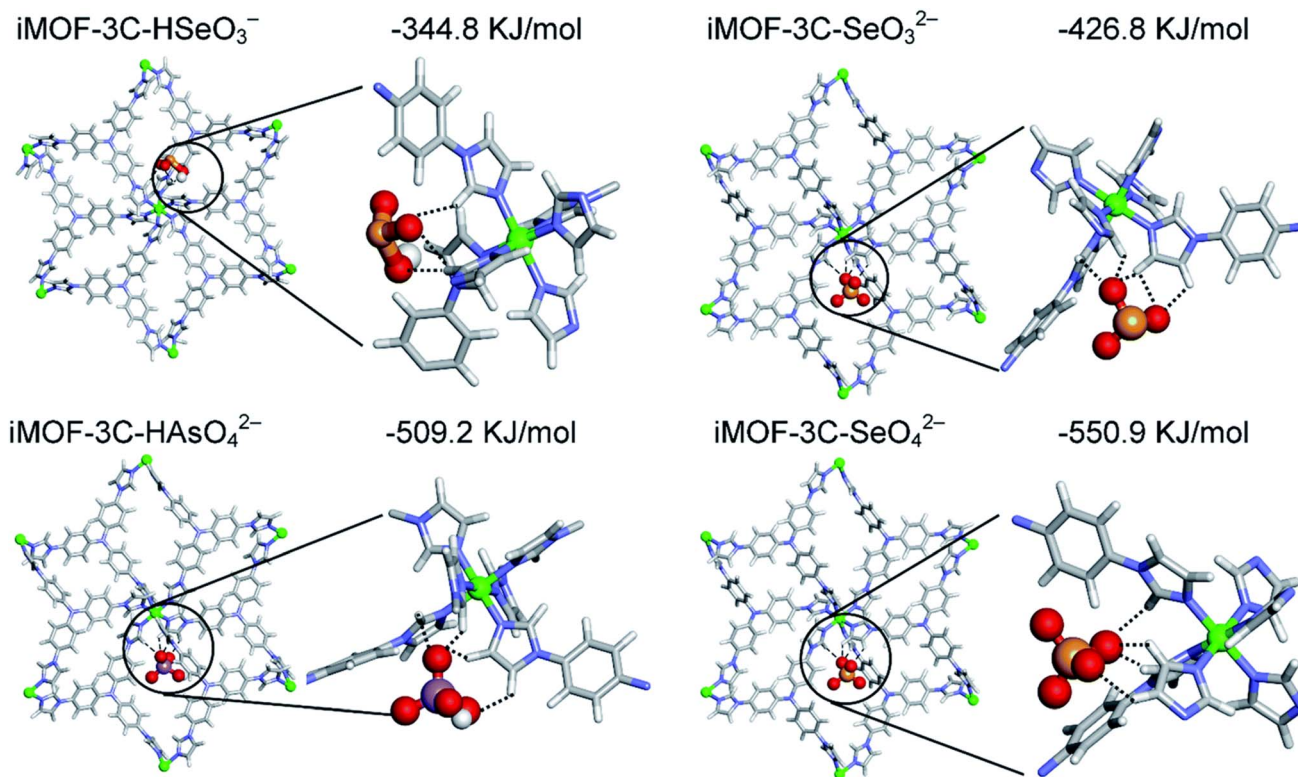
Fig. 10 DFT-optimized structures and corresponding magnified views showing the hydrogen bonding interactions of iMOF-3C with different oxyanions and binding energies (reproduced with permission from ref. 134).

3.3 Removal of pesticides using MOF

Pesticides are chemicals that are used to kill or control pests such as insects, rodents, weeds, fungi, bacteria, and other organisms that can damage crops and cause diseases. Pesticide pollution is the spread of pesticides to areas outside of their intended use, affecting land, water, air, wildlife, and human health. Pesticides can be carried by wind, rain, or runoff,

Table 1 Application of MOFs in the removal of metal ions[a]

MOF	Metal	Adsorbate/metal ion	Ce (mg g^{-1})	pH	Regeneration/cycles	Adsorption mechanism	Ref.
UiO-66-EDA	Zr	Pb(II)	243.9	—	04	Electron exchange, electron sharing, electrostatic and covalent interaction	113
		Cd(II)	217.3				
		Cu(II)	208.33				
ZIF-8	Zn	As(V)	76.5	4	Reusable	Inner sphere complex	135
MIL-53	Fe	As(V)	21.27	5	Reusable	Lewis acid–base and electrostatic interaction	136
MIL-53	Al	As(V)	105.6	8	Reusable	Electrostatic attraction, hydrogen bond	136
UiO-66	Zr	As(V)	303.34	2	Reusable	Ion exchange	137
Cubic ZIF-8	Zn	As(III)	122.6	8.5	Reusable	Ion exchange	138
β-MnO$_2$@ZIF-8	Zn	As(III)	140.27	7	Reusable	Oxidation	139
UiO-66-SH	Zr	Hg	785	4	Reusable	Interact with thiol	140
TMU-32S-65%	Zn, urea	Hg	1428	—	Reusable	Electrostatic interaction, chelation	141
MIL-53(Al) MFC	Al	Pb	492.4	—	Reusable	Ion exchange	142
MIL-101/GO	Fe	Pb	128.6	6	4 cycles	Ion exchange	114
UiO-66-RSA	Zr	Pb	189.8	4	Reusable	Complexation	143
NH$_2$-functionalized MOFs	Zr	Cd	177.35	6	Reusable	Coordination interaction	144
PAN/chitosan/UiO-66-NH$_2$	Zr	Pb	441.2	6	5	Chelation	115
		Cd	415.6				
		Cr	372.6				

[a] Ce = adsorption capacity.

contaminating natural resources and food sources. Pesticide exposure can cause intoxication, harm, and even death to living organisms. Pesticide pollution is a widespread and growing problem in many countries.[145] The excessive use of pesticides in agriculture to protect crops from pests, *etc.* results in the exposure of non-target vegetation to pesticides and they remain as pesticide residue in the environment and ecosystem. Pesticide residues in food matrices are one of the most urgent problems globally, posing a threat to the survival and growth of humanity.[146]

In recent years, MOFs have been successfully used for the detection and adsorption of pesticides, where various interactions are responsible for the adsorption of pesticides by MOFs (Fig. 11). An Fe₄O₃–graphene oxide (GO)–β-cyclodextrin (CD) nanocomposite was used as the magnetic core and support for a novel magnetic copper-based M-MOF, which was used for the adsorption and removal of neonicotinoid insecticide contaminants from aqueous solution.[147] Fe₄O₃-GO-βCD was found to be made up of a thin single layer with anchored Fe₃O₄ based on the characterization of M-MOF. On the surface of Fe₄O₃-GO-β CD, M-MOF was coated. The findings indicated that the produced M-MOF is an easy, efficient, and potential adsorbent for removing neonicotinoid insecticides from environmental waters.

A chrysanthemum-like Zn-BTC-based MOF and its application for pesticide adsorption from real water samples were explored.[148] The MOF was used to extract six aromatic pesticides from different wastewater samples *via* dispersive solid-phase extraction before HPLC quantification. The MOFs exhibited high chemical stability and attractive longevity due to the chemical bonding between BTC and Zn. These Zn-BTC MOFs as supports may be one of the most promising candidates for pollution separation and enrichment in the environment.

The preparation of CeO₂ nanofibers derived from a Ce-BTC MOF was reported, and the affinity of CeO₂ for pesticide 2,4-dichlorophenoxy acetic acid (2,4-D) was investigated.[149] Ce-BTC nanoparticles were synthesized using a hydrothermal process and calcined to generate CeO₂ nanofibers. It was found that the optimal amount of adsorbent was 2.5 mg and the best contact time was 100 min, resulting in the maximum adsorption capacity of 86.16 mg g^{-1} for 2,4-D at 298 K.

Eight organophosphorus pesticides were successfully isolated from environmental water and soil samples using the functional adsorbent of ZIF-8/magnetic multi-walled carbon nanotubes (M-M-ZIF-8).[150] Employing the coordination-polymerization technique, ZIF-8 particles were deposited on the surface of magnetic MWCNTs. Then, 15 mg of M-M-ZIF-8
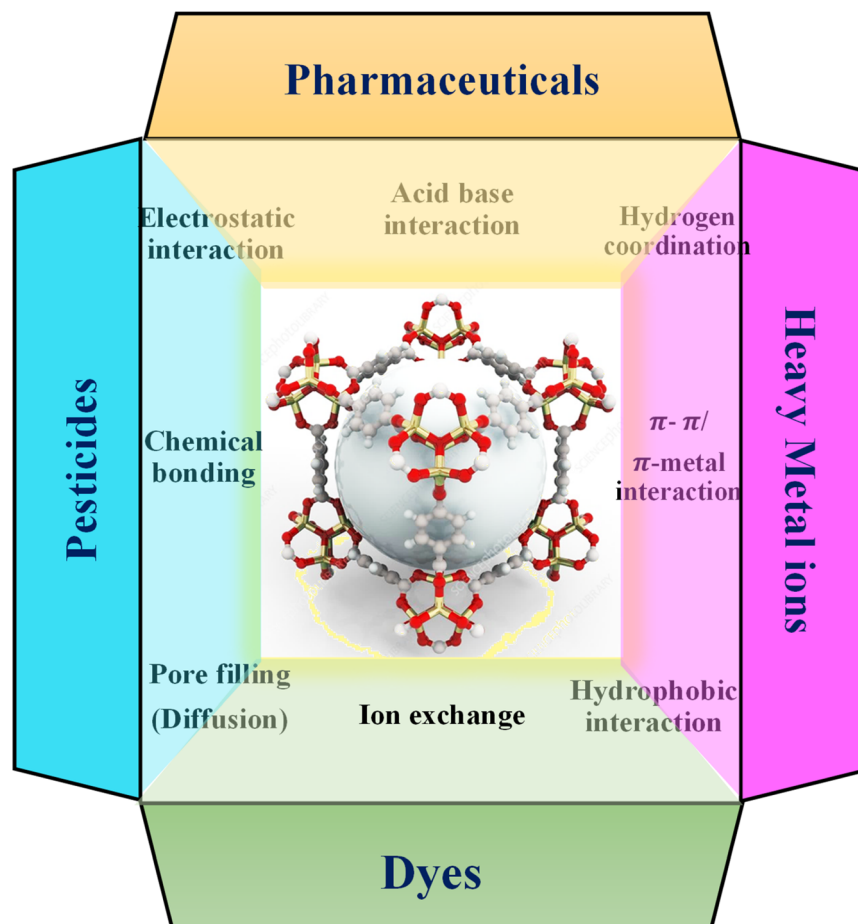

Fig. 11 Various interactions simultaneously occurring during the removal of pollutants from wastewater using MOFs.

was dispersed in 4 mL of aqueous solution maintained at pH 4 within eight organophosphorus pesticides at a concentration in the range of 0.2 to 8 mg L^{-1} and allowed to incubate for 15 min at room temperature. The resultant adsorbent M-M-ZIF-8 was magnetically removed followed by the determination of pesticide concentration in the supernatant by HPLC-MS-MS. The adsorption capacities of M-M-ZIF-8 (8 mg L^{-1}) for triazophos, diazinon, phosalone, profenofos, methidathion, ethoprop, sulfotep, and isazofos were reported to be 3.12, 2.59, 3.80, 3.89, 2.34, 2.18, 2.84, and 3.00 mg g^{-1}, respectively. The valence-electron-driven adsorption, in which the organophosphorus pesticide molecules share or exchange electrons with the vacant active sites of M-M-ZIF-8, is one possible mechanism proposed for the adsorption.

In one study, polyethylene terephthalate (PET) bottles were used as a source and support for the growth of UiO-66 MOF, which was used to extract imidacloprid from water.[151] PET@UiO-66 demonstrated excellent stability during the sorption process and could be recycled up to five times. The proposed technology demonstrates a novel opportunity for the reuse of PET waste in the development of recycled products that can be used to resolve environmental concerns.

The present study aimed to reveal the ability of the special porous structure of Basolite Z-1200 to adsorb and sense mecoprop pesticide.[152] The above-mentioned MOF was treated with mineral acid (HCl) to make it electrically active. Proton doping decreased the overall resistance of the MOF, according to the electrical measurements. Environmental sensors, preconcentration, solid-phase extraction, and electronic devices can all benefit from conducting MOF thin films.

Using a single layer of Fe$_3$O$_4$-ZIF-8 as the magnetic core and a layer of ZIF-67 as the outer layer, a novel MOF (M-ZIF-8@ZIF-67) was successfully prepared.[153] This M-ZIF-8@ZIF-67 adsorbent was used to adsorb and extract fipronil and its metabolites from water, exhibiting high adsorption potential according to the adsorption experiments. The maximum adsorption capacities for fipronil desulfiny, fipronil, fipronil sulfide, and fipronil sulfone in the solution supernatant, as determined by HPLC-MS/MS, at 10 mg L^{-1}, were 3.244, 3.955, 5.188 and 5.729 mg L^{-1}, respectively. The proposed mechanism is the bilayer structure of the ZIF-8@ZIF-67 composite material exhibits numerous similar pore structures, which enhance the adsorption and removal of organic pollutants. The adsorption data well-fitted the Freundlich adsorption isotherm rather than the Langmuir adsorption isotherm.

A super-hydrophilic graphene oxide/electrospun cellulose nanofibre (GO/CNF) was synthesized, characterized, and successfully used as an adsorbent in a solid-phase membrane tip adsorption (SPMTA) to analyze polar organophosphorus pesticides (OPPs) in multiple foods and water samples.[154] According to the adsorption results, a higher initial pH value influenced the adsorption capacity. In the OPP study, the newly synthesized GO/CNF-10 wt% showed great promise as an adsorbent with the maximum adsorption capacity for methyl parathion, ethoprophos, sulfotep, and chlorpyrifos of 0.039, 0.221, 0.075 and 0.069 mg g^{-1} respectively.

MIL-10[Fe] and NH$_2$-MIL-101[Fe] were both prepared using a simple process.[155] Due to the presence of an amine group, the adsorption kinetics and isotherms showed that NH$_2$-MIL-101[Fe] has higher adsorption ability than MIL-101[Fe] of 9.58 and 9.28 mg g^{-1}, respectively, following a pseudo-second-order model with chemisorption as the rate-limiting step. In addition, the Fe-based MOFs had high selectivity for phosphate in the presence of other anions including chloride, bromide, nitrate, and sulfate.

A novel MOF, i.e., UiO-67/GO nanocomposite, was successfully prepared and applied as a high-capacity adsorbent for glyphosate from polluted water.[156] UiO-67/GO was composed of dense and ordered UiO-67 on the surface of GO for high-affinity pesticide capture (OPPs). This study indicated that the UiO-67/GO composite has great potential as a next-generation adsorbent for water purification, owing to its excellent glyphosate-adsorption capability of 482.69 mg g^{-1} at pH 4. It also provided interesting opportunities for fabricating other MOF/GO for the successful removal of organic pollutants.

3.4 Removal of pharmaceuticals using MOFs

Pharmaceutical pollution is the pollution of the environment with pharmaceutical drugs and their metabolites, which reach the aquatic environment (groundwater, rivers, lakes, and oceans) through wastewater.[157] These drugs are biologically active substances specifically designed to cause pharmacological effects in living organisms. Thus, they have a significant impact on the health of wildlife and ecosystem when they are not treated in an environmentally friendly manner.[158]

Nowadays, the global consumption of drugs, whether prescribed or influenced by social media, is increasing tremendously. Ultimately, this has led to the disposal of drugs and their metabolites into water bodies, generating a major source of water pollution given that they directly/indirectly influence the sources of drinking water and the food chain. One of the most significant impacts of environmental residues of pharmaceuticals is the development of antimicrobial resistance (AMR).[158] Pharmaceutical pollutants include carbon monoxide, particulate matter, volatile organic compounds, carbon dioxide, methylene chloride, methanol, toluene, and hydrogen chloride. They also include medicinal products, skincare and hygiene products, insecticides, detergents, organic mordants, and habitual industrial organic chemicals such as phenolic halogens and aromatics.

The effectiveness of the removal of these microcontaminants is significantly influenced by the physicochemical properties of the contaminants (e.g., pK_a, functional groups, and hydrophilicity). The removal of the contaminants of environmental concern is detailed and reviewed elsewhere.[69,71,159]

The synthesis of a perfluorinated in-derived MOF, YCM-101, was reported using InCl$_3$ and tetrafluoroterephthalic acid. It exhibited the capability to remove the antibiotic tetracycline from aqueous solution via the induced π–π stacking interactions between the MOF linker and tetracycline with a maximum adsorption capacity of 32 mg g^{-1}.[160] Here, YCM-101 was reported as the first indium-derived perfluorinated MOF in the literature, which is a 3-dimensional neutral MOF containing an

$[In(\mu-O_2CR)_2(\mu-OH)]_\infty$ infinite chain secondary building unit (SBU), where each bridging organic ligand is linked to two distinct SBUs. However, YCM-101 was found to be unstable upon the complete removal of solvent from the pores, given that its BET surface areas ranging from 50 m² g⁻¹ to 200 m² g⁻¹ were inconsistent and irreproducible.

MIL-101 with and without functionalization was reported for the adsorptive removal of nonsteroidal anti-inflammatory drugs (naproxen and ibuprofen) and oxybenzone, which is an integral component of many sunscreen lotions.[161] The porosity of the synthesized MIL-101 was reduced after the introduction of –OH, –NO₂, and –NH₂ functionalization. The maximum adsorption capacity exhibited by MIL-101-OH for naproxen was 185 mg g⁻¹. For the adsorption of naproxen on MIL-101 in aqueous media, the carboxylic acid and ether functional groups of naproxen and the –OH and –NH₂ on MIL-101 played a significant role (via electrostatic interactions), which can be used as H-donors in H-bonding, whereas MIL-101 modified with H acceptors did not act as a good adsorbent for naproxen. The adsorbed amount at equilibrium decreased in the order of MIL-101-OH > MIL-101-NH₂ > MIL-101-(OH)₂ > MIL-101 > MIL-101-NO₂, which was the same order observed for the quantity adsorbed after various times.

Luo et al.[66] reported the synthesis of a Cu-based 3-D MOF, H5L, decorated with carboxylate as an adsorbent for diclofenac sodium and chlorpromazine hydrochloride from water. In this study, the effect of basic parameters (pH, initial conc, time, temp, and dosage of adsorbent) on the adsorption capacity of 3-D MOF was evaluated. The studies indicated comparatively higher uptake for diclofenac sodium (following Langmuir model and pseudo-first-order kinetics) compared to chlorpromazine hydrochloride (followed Temkin model and pseudo-second-order kinetics), suggesting the weak interaction between the uncoordinated –COO– groups of the host MOF and drugs.

The adsorption and removal characteristics of MOFs for clofibric acid from medicinal materials and personal care products were explored.[162] Specifically, MIL-101[Cr] and MIL-101-OH were synthesised and modified by adding hydroxyl functional groups (–OH) to MIL-101 and used in the analysis (Cr). MIL-101[Cr] possessed a higher surface area than MIL-101-OH, but MIL-101-OH had slightly better clofibric acid adsorption performance than MIL-101[Cr] (based on unit weight). In another report,[163] researchers have described the adsorption and degradation of Amox by ZIF-8 and Zn(1,4-benzene dicarboxylate) (ZnBDC). The degradation of Amox was attributed to the catalytic action of the Zn²⁺ ion in mono- and binuclear metallo-β-lactamases, which are often tetra-coordinated with imidazolate rings from histidine residues acting as ligands. Upon the exposure of Amox to ZIF-8 and ZnBDC, the non-toxic penicilloic and penilloic acids were formed as the degradation products.

Non-steroidal anti-inflammatory drugs (NSAIDs) are the most extensively utilized pharmaceutical anionic aromatic compounds with stable structures, high polarity, and water solubility. However, the complete removal of these drugs from water bodies is a challenging task using conventional water treatment methods. Therefore, alternative methods are required for their degradation and entrapment from water resources. In this case, MOFs represent a promising class of porous and functional materials for the adsorptive removal of NSAIDs. In one study,[164] UiO-66, MOF 808, and MOF 802 were explored for the removal of NSAIDs from groundwater, surface water, and wastewater. Various sophisticated instrumental techniques (energy-dispersive X-ray, powder X-ray diffraction, field-emission scanning electron microscopy, N₂ adsorption and desorption isotherm measurements, pore size distributions of the MOFs by nonlocal density functional theory (NLDFT) model, HPLC, and XPS) were employed to explore the interaction between the NSAIDs and MOFs. Besides, the binding energies of the NSAIDs in the MOFs were also investigated by DFT calculations using the DMol3 tools in Material Studio 7.0 (Accelrys Software Inc). Based on the experimental characterization, the adsorption mechanism was attributed to the chemical adsorption and high electrostatic interaction between the incompletely coordinated cationic Zr in the cluster and anionic NSAIDs (carboxyl groups) in combination with the pi–pi interaction between the benzene ring of the NSAIDs and MOF ligand. The adsorption capacity of UiO-66 and MOF-808 can be regenerated successfully for up to three cycles.

In another study,[165] solvothermally synthesized MIL-53[Fe] was explored (as a function of initial drug concentration, adsorbent dose, and pH) for the adsorption of ibuprofen in synthetic solution. More than 80% of 10 mg L⁻¹ ibuprofen was claimed to be eradicated by the chemisorption and monolayer formation adsorption process. In a recent study,[159] chitosan-alginate-based micro composite beads of aluminum, MIL-68[Al] (built from infinite chains of octahedral AlO₄(OH)₂ linked through terephthalate ligands), were explored for removal of bisphenol A from wastewater and showed excellent adsorptive behavior compared to their analogous components. The adsorption mechanism was mainly established by H-bonding, cation–pi interaction, and pi–pi stacking, as confirmed by the characterization studies. These micro composite beads could be employed in five successful regeneration cycles with almost 95% adsorption capacity.

In another study,[166] two MOFs (MIL-100[Fe] and MIL-101[Cr]) synthesized via the solvothermal method were reported as ultrafiltration (UF) hybrid systems to remove ibuprofen (a common pain killer) and 17α-ethinyl estradiol (a synthetic hormone) together with some other natural organic matter. The MOF showed a 53.2% retention rate for pharmaceuticals compared to only 36.7% by UF. The size effect, electrostatic interaction, and hydrophobic interaction were considered as the three mechanisms for the adsorption of the drug by the studied MOFs. However, due to the larger surface area and pore volume of MIL-101[Cr], it showed a higher adsorption capacity under all the experimental conditions. The retention rates of ibuprofen and 17α-ethinyl estradiol followed the order of UF only < MIL-100[Fe]-UF < MIL-101[Cr]-UF, which was significantly influenced by the pH of the adsorption medium.

In another study, MIL-101 [Cr] and MIL-101[OH][167] synthesized by the hydrothermal method were used as adsorbents for clofibric acid (a bioactive metabolite of various lipid-regulating

pro-drugs and a metabolite of the cholesterol-lowering pharmaceutical drug clofibrate). MIL-101[OH] was functionalized, following the grafting method by dehydrating MIL-101[Cr] at 150 °C for 12 h in a vacuum oven. The batch adsorption studies were found to follow Langmuir adsorption isotherm and pseudo-second-order kinetics. The maximum adsorption capacity observed with MIL-101 [Cr] and MIL-101[OH] was 357 and 385 mg g^{-1}, respectively. However, despite the lower surface area and pore size of MIL-101[OH], it showed a higher adsorption capacity for clofibric acid compared to the pristine MIL-101[Cr] due to the presence of H bonding, π complexation between MIL-101 and benzene ring of the adsorbate, and acid–base interaction due to the interaction between the modified MOF with –OH groups with the sorbates –COOH groups.

In a recent study,[168] the MIL-125[Ti]/MIL-53[Fe] binary MOF was incorporated with carbon nanotubes (CNTs) in alginate (Alg) microbeads to form MIL-125[Ti]/MIL-53[Fe]/CNT@Alg composite microbeads for the removal of tetracycline from wastewater. The synthesized microbeads were found to possess a high specific surface area of 273.77 m^2 g^{-1} with a maximum adsorption capacity of 294.12 mg g^{-1} at 25 °C and pH 6. The MIL-125[Ti]/MIL-53[Fe]/CNT@Alg composite microbeads retained excellent adsorption capacity for six consecutive cycles. Besides, the π–π interaction between the aromatic rings in MIL-125[Ti]/MIL-53[Fe]/CNT@Alg (π-electron donor) and TC molecules (π-electron acceptor) was dominant in the proposed mechanism for TC adsorption by the pore filling effects attributed to the three dimensions of the TC molecules (length, width, and height of 1.23, 0.84 and 0.67 nm, respectively), which can easily accumulate in the synthesized microbeads with an average pore size of 2.145 nm.

In another study,[169] a binary MOF of Fe and Cu, i.e., MIL-53, was synthesized via a single-step solvothermal route for the adsorption and photocatalytic degradation of ciprofloxacin with a maximum adsorption capacity of 190.40 mg g^{-1} and a maximum degradation of 74.48% and 57.88% in the presence of UV and visible radiation, respectively. The photoluminescent spectra confirmed that the synthesized MIL-53[Fe–Cu] possessed longer photocatalytic activity due to the structural defects caused by the presence of Fe and Cu in the MOF, which led to a low rate of photogenerated electron and hole recombination. The adsorption capacity of MIL-53[Fe–Cu] was found to be about 51% after five regeneration cycles.

In another study, the adsorption properties of the CuBTC@NH$_2$ MOF composite were examined for pharmaceutical contaminants.[170] The physicochemical properties of the MOF were significantly enhanced by the post-synthetic alteration of CuBTC@NH$_2$, which resulted in differences in the adsorption behavior for pharmaceutical pollutants such as ibuprofen (IBF) and acetaminophen (ACE) from aqueous solutions. It was obvious that the CuBTC@NH$_2$ MOF successfully removed pharmaceutical impurities through chemisorption. Due to the electrostatic and hydrophobic interactions, the pH of the solution had a significant impact on the adsorption of pharmaceutical contaminants. The total adsorption capabilities for IBF and ACE were 187.97 and 125.45 mg g^{-1}, respectively. The outcomes demonstrated that the created nanocomposite

can effectively treat polluted effluents by eliminating IBF and ACE from aqueous fluids. Some studies for the adsorptive removal of pharmaceuticals are presented in Table 2.

4. Photocatalytic degradation of pollutants using MOFs

Photocatalysis is one of the most promising techniques to achieve environmental remediation and address related concerns. In this process, the photocatalyst utilizes renewable solar energy and creates a strong oxidizing agent, which completely breaks down the organic pollutants present in air or water bodies into non-toxic inorganics such as water and carbon dioxide without causing secondary pollution.[172–174] Moreover, they can be used in both liquid and gaseous media such as TiO$_2$,[175,176] ZnO,[177] CdS, and g-C$_3$N$_4$.[178] These impressive properties of photocatalysts have prompted researchers to develop a variety of photocatalytic materials. Over the last two decades, a variety of photocatalysts have been synthesized and their application in the degradation of organic pollutants investigated.[179–181]

The mechanism of photocatalysis is based on the energy difference between the valence band and the conduction band of materials. Upon the irradiation of a photocatalyst with solar energy above its band gap, the electrons present in its valence band get excited to the conduction band, while holes remain in the valence band. This paves the way for various oxidation and reduction reactions to occur.[182] However, these photocatalysts often exhibit limited practical applications in environmental remediation and low photocatalytic efficiency. This is attributed to the low availability of electrons and holes for oxidation–reduction reactions due to the rapid recombination of photogenerated electron–hole pairs.[183] Therefore, exploring novel photocatalysts has attracted significant attention.

In the last few years, MOFs have been recognized as pioneering photocatalysts due to their unique characteristics such as uniform distribution of pore channels, considerable chemical, thermal and mechanical stability, dual active sites, high surface area, and recyclability. They were first used as a semiconductor for the degradation of phenol in the presence of UV light.[184] Since then, they have been applied in various photocatalytic systems, especially the remediation of organic pollutants present in the environment. The diverse remarkable features of MOFs such as tunable active sites (such as organic linkers and metal–oxygen–carbon clusters), the modular nature of their synthesis, tailorable electronic nature, and topological structure having dispersed active sites to avoid agglomeration make them highly fascinating for use in photocatalysis. Furthermore, the chromophores of organic linkers can be tailored to maximize the utilization of solar energy. For example, Nasalevich et al. utilized amino chromophores to shift the absorption edge to the visible region of the spectrum.[185] Recently, Gheytanzadeh and group reported the use of artificial intelligence techniques in the photocatalytic degradation of tetracycline using MOFs.[186] The tetracycline degradation was measured using the Gaussian process regression (GPR) model

Table 2 Removal of pharmaceuticals using MOFs

S. no	MOF	Metal	Adsorbate	Adsorption capacity	Mechanism	Remark	Ref.
1	YCM-101	Ir	Tetracycline	32 mg g^{-1}	π–π stacking interactions between an MOF linker and tetracycline	Efficient for 3 runs	160
2	MIL-101	Cr	Naproxen, ibuprofen, oxybenzone	185 mg g^{-1}	H bonding	Several runs	161
3	MOF1	Cu	Diclofenac sodium Chlorpromazine HCl	0.49 g g^{-1} 0.29 g g^{-1}	Weak interaction between uncoordinated –COO– groups of host MOF1 and drugs	After 200 min of stirring, about 85% of diclofenac sodium and 60% of chlorpromazine hydrochloride can be desorbed	66
4	ZIF-8	Zn	Amoxicillin	—	Amox adsorbs to framework through electrostatic interactions between its carboxylate groups and the Zn^{2+} metals in the material surface	Nontoxic degradation products formed, *i.e.*, penicilloic and penilloic acids	163
5	MIL-101(Cr) and MIL101-OH	Cr	Oxybenzone	73.5 mg g^{-1} and 121 mg g^{-1}	H-bonding	—	171
6	UiO-66 MOF 808 MOF-802	Zr	Ibuprofen Ketoprofen Naproxen Indomethacin Furosemide Salicylic acid Acetophenone Amitriptyline	141 L mmol^{-1}	π–π stacking interactions, chemical adsorption	High binding energy (-300 kJ mol^{-1}), the synergistic effect of chemical adsorption for high adsorption of nonsteroidal anti-inflammation drugs	164
7	MIL-53 SA= (5.5 m^2 g^{-1})	Fe	Ibuprofen	80% of 10 mg L^{-1} drug	Chemisorption	—	165

having four kernel functions by changing the MOF features with different parameters such as pore volume, surface area, and other operational parameters such as concentration of tetracycline, catalyst dosage, illumination time and pH.

4.1 Mechanism of MOF-photocatalyzed degradation of organic pollutants

During the photocatalytic process using MOFs, the organic linker having a functional chromophore acts as an antenna and absorbs the radiation from the light source. Upon irradiation, the loosely held electrons present in the chromophore absorb energy and get excited to the highest occupied molecular orbital (HOMO) energy level. These excited electrons transfer their energy to metal-oxo clusters.[187] This is known as the ligand-to-metal charge transfer (LMCT) mechanism and is most commonly used in the MOF-based photocatalytic degradation process.[185] In addition to the LMCT mechanism, other mechanisms such as metal-to-ligand charge transfer, ligand-to-ligand transfer, and metal-to-metal-to-ligand charge transfer (in case of more than one metal) have also been used to elucidate various photocatalytic activities.[173] Besides these mechanisms, some metal clusters such as Fe–O clusters (Fe-based MOFs) tend to absorb light and get photoexcited directly to generate electrons and holes.[187] In the latter case, the oxygen molecules present in the metal cluster capture the photogenerated electrons and get converted to superoxide radicals ($O_2^{\cdot-}$). Alternatively, the photogenerated holes formed on the HOMO orbital (due to the transfer of electrons to LUMO) possess strong oxidizing ability. Due to this ability, these holes degrade organic pollutants directly by oxidation and also react with water molecules to form hydroxy radicals, another oxidizing species.[188] All three key active species generated during this process, *i.e.*, superoxide radicals, holes, and hydroxy radicals, possess super oxidizing power. Hence, these MOFs have a remarkable ability to completely decompose the organic pollutants present in the environment into non-toxic inorganic molecules such as carbon dioxide and water molecules without causing further pollution. However, the mechanism may vary depending on the type of pollutant and the energy band pattern of the photocatalyst.

Considering the above-mentioned mechanisms, some strategies can be applied to increase the efficiency of MOFs as photocatalysts. More effective chromophores having excellent light absorbing tendency can be substituted in their organic linkers together with the choice of suitable metal centers to increase the absorption of light, and hence greater photocatalytic efficiency can be achieved from the designed MOFs. Moreover, the recombination of photogenerated electrons and holes can be reduced by tailoring the functionalization of MOFs as well as by the addition of an external electron acceptor. The latter results in increased production of hydroxy radicals, leading to a sharp enhancement in the photocatalytic activity of MOFs. Furthermore, the effective capture of target pollutants on the open pore active sites of MOFs confines the concentration of adsorbed pollutants in the microenvironment, and hence they can stay for longer to complete the process of degradation, ultimately leading to better efficiency of MOFs as photocatalysts.[189]

4.2 Types of metal-MOFs for photocatalytic applications

4.2.1 Co- and Ni-based MOFs. Co- and Ni-based MOFs have been widely used as efficient photocatalysts for the degradation of organic pollutants. Wen *et al.* synthesized a variety of Co- and Ni-based MOFs, $[M(btec)_{0.5}(bimb)]_n$ having 4,4′-bis(1-imidazolyl)biphenyl (bimb) and 1,2,4,5-benzene tetracarboxylic acid (H_4btec) as organic linkers, using the solvothermal method.[190] The structural characterization revealed that Co-MOF possessed a 3D structure, while Ni-MOF possessed a 2D layer network. Both MOFs were thoroughly characterized using various techniques. They were found to be unusual examples of visible light-active photocatalysts with excellent photocatalytic activity towards the degradation of the anionic organic dye X3B. X3B is an organic dye that is known to be very difficult to decompose under UV and visible light irradiation. Both Co- and Ni-based MOFs showed remarkable photocatalytic activity of 90% and 80% in 9 h towards the degradation of X3B. They also showed the effect of the addition of hydrogen peroxide (H_2O_2) as an electron acceptor in the degradation process. The same photocatalytic efficiency was observed in just 5 h in the presence of H_2O_2. Many researchers have reported a variety of other Co- and Ni-based MOFs as efficient photocatalysts for the decomposition of organic pollutants without causing secondary pollution. In recent years, nickel/cobalt bimetallic MOFs have been used as electrocatalysts for the oxygen evolution reaction (OER). Sondermann *et al.* used a bimetallic (or mixed metal) MOF, Ni_{10}Co-BTC (BTC = 1,3,5-benzene dicarboxylate), which acted as a sacrificial agent as some structural changes occurred to form $NiCo_2O_4$ during the electrochemical measurements. The stable mixed metal species obtained were shown to produce good results in the OER studies.[191]

4.2.2 Ni-, Co- and Zn-based MOFs. Natarajan *et al.* extensively used a series of MOFs having metal ions Co, Ni, and Zn as photocatalysts to degrade the most commonly used organic dyes such as methylene blue (MB), rhodamine B (RhB), brilliant blue R (BR), and orange G (OG).[192] It was found that the efficiency of these MOFs for the degradation of all of these dyes decreased with an increase in their energy band gap values. Later, many researchers conducted kinetic studies to correlate the mechanism of action of these MOFs in heterogeneous photocatalytic degradation using a variety of metals as a structural platform for MOFs with different organic dyes.[193,194]

4.2.3 Zn-based MOFs. In 1999, Li and co-workers synthesized MOF-5 using zinc nitrate, 1,4-BDC, chlorobenzene, and DMF, which has the formula $Zn_4O(BDC)_3 \cdot (DMF)_8 \cdot (C_6H_5Cl)$.[195] The structural elucidation showed the presence of Zn_4O clusters at the corners of the cubic framework, having an orthogonal connection by 1,4-BDC ligand. Further, in 2007, for the first time, the photocatalytic activity of MOF-5 was examined for the degradation of phenol in an aqueous solution by Garcia and group. MOF-5 showed a broad absorption band in the region of 500–840 nm with a bandgap of 3.4 eV and found to be as efficient as commercial TiO_2, which established MOF-5 as

a remarkable photocatalyst.[196] According to the proposed mechanism, electron transfer takes place from phenol to the MOF holes through the absorption of light, which leads to the generation of oxygen-active species. These active oxygen species are capable of oxidizing organic pollutants to non-toxic molecules.

Interestingly, MOF-5 was found to be more efficient than ZnO and TiO_2 for the photocatalytic degradation of waste organic contaminants given that it absorbs visible light and shows a broad absorption spectrum in the visible range. Furthermore, Garcia *et al.* continued their work on MOFs and studied the shape-selective photocatalytic degradation efficiency of MOF-5 towards different organic compounds. They compared the photocatalytic efficiency of MOF-5 towards the degradation of small-sized phenol and large-sized 2,6-di-*tert*-butylphenol (DTBP) molecules in a mixture. It was determined that phenol molecules, being smaller in size, can easily diffuse into the micropores of MOF-5, and hence not much is available on the surface of MOF-5, which results in a lower rate of photocatalytic degradation. Alternatively, DTBP molecules, being larger remain on the external surface of MOF-5 and undergo photocatalytic degradation at a much higher rate. However, MOF-5 showed comparable efficiency towards the degradation of both molecules when exposed to UV light individually. Hence, they inferred that the selective photodegradation of DTBP molecules over phenol molecules using MOF-5 as a photocatalyst.

Chen and coworkers reported the synthesis of double-layered porous Zn-MOF UTSA-38 having the formula $[Zn_4O(2,6-ndc)_3(DMF)_{1.5}(H_2O)_{0.5}]_4(DMF)\cdot7.5H_2O$ and used it for the photocatalytic degradation of methyl orange (MO).[197] The degradation study was carried out in both the visible and UV light range. The photocatalytic efficiency was found to be much higher upon UV light irradiation compared to that under visible light. The mechanism of action of Zn-MOF UTSA-38 involved the absorption of UV radiation by its organic linker followed by the migration of photogenerated electrons and holes to the surface of UTSA-38. The hydroxy radicals generated during the reduction of oxygen decompose the MO dye into non-toxic water and carbon dioxide molecules. After completion of the process, the photocatalyst Zn-MOF UTSA-38 was recovered by simple filtration and used for further reactions after reactivation (through repeated washing and drying processes). A variety of Zn-based MOFs was synthesized and studied for the photocatalytic degradation of organic pollutants under UV and visible light irradiation.[198] Recently, Herrera and group reported the synthesis of the Zn-BDC MOF having structural similarity with MOF-5 and explored a combination of its applications including adsorption capacity, kinetic adsorption and pH effect, and hydrogen evolution using dyes, namely, MO and MB.[199] They concluded the better photocatalytic activity of Zn-BDC MOF suspended in a solution of methylene blue dye for the evolution of hydrogen.

4.2.4 Cd-based MOFs. In addition to the most commonly used Ni-, Co- and Zn-MOFs, several Cd-based MOFs have also been reported in the literature for their efficiency towards photocatalytic degradation of various organic pollutants such as

MO, MB, RhB, and X3B.[200,201] The various Cd-MOFs include $Cd(btec)_{0.5}(bimb)_{0.5}$, $[Cd(4,4'-bpy)(H_2O)_2(S_2O_3)]\cdot2H_2O$, $Cd(4-bpah)(1,3-bdc)(H_2O)$ and $Cd_2(4,4'-bpy)_3(S_2O_3)_2$. Kaur and co-workers synthesized a visible light-active Cd-MOF, $[Cd(2-ATA)(4,4'-bpy)]_n$, using 2-aminoterephthalic acid and bipyridine as organic linkers and used it for the photocatalytic degradation of methylene blue dye in the presence of a visible light source of radiation.[202] It showed 82% photocatalytic efficiency within only 90 min. In continuation of their work, another Cd-MOF, $[Cd(PA)(4,4'-bpy)_2](H_2O)_n$, was synthesized using pamoic acid and bipyridine as organic linkers.[203] This MOF was tested for the complete removal of a variety of organic pollutants such as RhB, MB, MO, and neutral red (NR) dyes and it showed good photocatalytic efficiency.

4.2.5 Ti-based MOFs. Titanium-based MOFs have gained an upsurge of interest from scientists in recent years due to their boosting efficiency towards the removal of pollutants. Recently, Zhao reported the use of Ti-MOF with MIL-125-NH-RSO_3H, where $R=CH_2CH_2CH_2$ as an adsorbent for the removal of metformin hydrochloride (Met·HCl) from contaminated water.[204] The anti-interference ability of the adsorbent in the presence of co-existing salts together with efficient host–guest interactions improved its performance in the decontamination of water. Liu *et al.* presented another example of the catalytic performance of a Ti-based MOF under visible light.[205] The heterojunction of TiO_2-carbon nitride as a photocatalyst was synthesized through the pyrolysis of a melamine mixture/NH_2-MIL-125 and studied for its photodegradation efficiency towards methylene blue and tetracycline. They reported the accelerated charge-transfer properties of the hybrid composite of Ti-based MOF and carbon nitride, and hence improved photocatalytic efficiency towards the removal of dye.

4.2.6 Other metal-based MOFs. Due to the remarkable photocatalytic efficiency and other wide applications of MOFs in the environmental remediation of organic pollutants, there is high demand for the synthesis of novel varieties of MOFs. In the recent literature, three Ag-MOFs including $[Ag_2(dpe)_{1.5}(sbdc)_{0.5}](sbdc)_{0.5}\cdot7H_2O$, $Ag_2(bpe)_2(npdc)\cdot2H_2O$ and $Ag_4(bpy)_4(ap)_2\cdot11H_2O$ were synthesized by Wang *et al.* using silver nitrate and organic linkers such as 1,2-di(4-pyridyl)ethylene, stilbene dicarboxylic acid, 2,6-naphthalene dicarboxylic acid, bipyridine (bpy) and 5-amino isophthalic acid.[206] The crystal structure of these MOFs showed an infinite 1D framework of silver-ligand cations and carboxylate anions, resulting in charge separation in their structure. These MOFs showed excellent photocatalytic activity towards the degradation of MB dye upon irradiation with UV light. Besides Ag-MOFs, a variety of other metal MOFs such as Pb, Zr, Hf, and Gd has also been reported to exhibit good photocatalytic efficiency in the decomposition of environmental organic contaminants.

Hf-based MOFs have also been used as an efficient heterogeneous acid–base catalysts for the transformation of biomass-derived furanic carbonyls. They can also be used for various organic transformations such as Meerwein–Ponndorf–Verley reduction and cross-aldol condensation through the acid–base pairs present in their framework.[207] These MOFs functionalized with Eu^{3+} have also been used for the fluorescence sensing of *p*-

nitrophenol and 3-methyl-4-nitrophenol as urinary metabolites present in organophosphorus pesticides.[208]

5. Application of MOFs in sensing water contaminants

The sensing of water contaminants including several ions, organic compounds, dyes, heavy metals, pharmaceuticals, and bacteria is necessary to address the problem of water pollution globally. Since their discovery in 1995 by Yaghi and coworkers,[209] MOFs have been proven as a promising sensing materials for the significant detection of water contaminants. The MOF-based sensors studied thus far rely on luminescence, electrochemical detection, colorimetric detection, and surface-enhanced Raman spectroscopic (SERS) detection.[210]

5.1 MOF-based luminescence sensors

Among the various available techniques to detect water pollutants, luminescence is the most widely used and considered advantageous because of its rapid, highly sensitive, cost-effective, and easy-to-operate conditions. In luminescence, light is emitted upon the absorption of energy. Fluorescence and phosphorescence are two basic phenomena of luminescence. To determine various analytes, there are two luminescent sensing mechanisms, *i.e.*, "turn on" and "turn off". In the "turn-on" mechanism, there is improvement in luminescence signal after adding the analyte, whereas the turn-off mechanism is based on the quenching of luminescence after adding the analyte. Although the turn-off phenomenon is more common in MOF-based sensors,[211] reports are also available on turn-on MOF sensors for water contaminants.[212] Numerous luminescence MOFs based on different luminescent mechanisms have been developed thus far to detect water pollutants.[213]

5.1.1 Sensing of nitroaromatic compounds.
Nitroaromatic compounds (NACs) are becoming a serious threat to water resources. Chun-Sen Liu and coworkers developed a dual-emission luminescent sensor based on an Eu-MOF composite for the selective detection of nitroaromatic compounds in water.[214] The synthesized sensor exhibited the luminescence properties of both Eu and the ligand. Their study indicated the retention of luminescent properties over a wide pH range (pH 4–11). The developed sensor was successfully used to detect acetone, dichromate ions, and various nitroaromatic compounds. Dichromate ions showed a significant quenching effect on the luminescent property of the ligand. The results indicated a slight enhancement in quenching efficiency with an increasing number of cycles. When applied to the detection of nitroaromatic compounds, the synthesized sensor showed different effects on different NACs. The luminescence was found to be fully quenched with tri-nitro phenol, while PNT showed the opposite effect to that of TNP. In addition to NB, the emission of Eu(III) was quenched significantly. This report suggested that the developed sensor can be used to successfully distinguish different nitroaromatic compounds. Moreover, the sensing probe was found to be reusable for up to 3 cycles. In another report,[215] a novel 3D water-stable luminescent sensor based on Zn-MOF, $\{[Zn(L)(bpe)_{0.5}]\cdot DMF\}_n$, was synthesized using the solvothermal technique. The synthesized sensor was employed successfully to detect trinitrophenol, nitrofurazone, and dichromate ions with improved sensitivity and selectivity in aqueous solution. Further, the potential of the sensor was investigated for tap water to demonstrate its detection ability in real-life environmental samples. Various water-stable Zn-MOFs with large surface areas were screened for the detection of dichromate ions in the water system and it was observed that NU-1000 is an excellent fluorescence sensor with a wide linear range and low detection limit.[216] Lu *et al.* designed and developed a tetrazole-based proton-conducing MOF fluorescence sensor for the determination of nitrobenzene in aqueous systems. Due to metal to metal-to-ligand transfer, the developed sensor exhibited green fluorescence for the detection of nitrobenzene.[217]

5.1.2 Sensing of heavy metal ions.
Heavy metal ions are regarded as major non-biodegradable water contaminants, which are highly poisonous even in small quantities. Therefore, the determination of heavy metal ions remains a prime concern for researchers and various luminescence MOF materials have been developed and investigated for sensing heavy metal ions and other cationic species.[213] Recently a stable and selective multifunctional 3D Eu^{3+}-based MOF luminescent sensor was developed for the detection of ferric ions, chromate ions, dichromate ions, and aspartic acid in water systems with a low detection limit.[218] Also, a non-luminescent MOF was converted into a luminescent MOF-based sensor. The developed sensor was used for the detection of lead in polluted water.[219] In another report, Vahid Safarifard used the solvothermal technique to prepare a Zr-based MOF as a luminescent sensor for the absorption of Hg^{2+} ions.[220] This sensor was highly sensitive and selective toward Hg^{2+}. It showed a good response time with the detection limit of 0.01 μm. Zhai *et al.* designed an Mg-MOF as a turn-off-turn-on luminescent sensing probe for Al^{3+}.[221] A trace level of Al^{3+} was detected even with the naked eye by the ratiometric color change. Previously, most MOF-based luminescent detectors were based on the turn-off mechanism; however, during the last decade, researchers have been working on the design and development of turn-on sensors for the detection of water contaminants. Sui-Jun Liu *et al.* reported Co(II)-MOF, a 3D structure having the formula $\{[Co_3(BIBT)_3(BTC)_2(H_2O)_2]\cdot solvent\}_n$, as the first turn-on fluorescent sensor for the simultaneous detection of Fe^{3+}, Cr^{3+} and Al^{3+} with a very low LOD.[222] The turn-on outcome of the sensor was attributed to the absorbance-caused enhancement mechanism. Li and Wang developed a 3D Cd coordination polymer-based MOF, a multi-responsive sensor with the formula $[Cd(Hcip)(bpea)_{0.5}(H_2O)]_n$,[223] for the turn-on ratiometric luminescence-based detection of aluminum and chromium ions. The developed sensing platform could also detect Fe^{3+} *via* a turn-off quenching effect. Based on the synthesized sensor, the authors designed simple and convenient luminescent test paper, which displayed a color change from green to blue with Al^{3+} and Cr^{3+} and colorless with Fe^{3+}. The experimental and theoretical investigations on the luminescent mechanisms suggested that Al^{3+} and Cr^{3+} may interact with the covalent Cd-CP framework, which can affect

the energy transfer. For luminescence quenching by Fe^{3+}, the overlapping of the absorption band of Fe^{3+} with the excitation band of the sensing material played an important role. In another report, Ghosh et al. fabricated a stable luminescent MOF using 2,5 pyridine dicarboxylic acid ligand and Zr^{4+}. The fabricated UiO-66@N was evaluated for the selective detection of Fe^{3+}.[224] Ghosh et al. also reported the synthesis of a water-stable luminescent cationic MOF, which exhibited a sensing response for Cr- and As-based oxo-anions in water.[225]

5.1.3 Sensing of inorganic ions. The nitrite ion (NO^{2-}) is considered to be a hazardous water pollutant. Recently, the research group of Wei Shi and Peng Cheng designed and synthesized a Tb-MOF sensor, $\{[Tb(CA)(OA)_{0.5}(H_2O)_2]\cdot H_2O\}_n$ (Tb-MOF), to determine nitrite ions in a water sample.[226] Fluorescence quenching was observed after the addition of nitrite ions. The sensing mechanism studies revealed dynamic quenching behavior owing to the transfer of energy from Tb-MOF to the nitrite ion. This sensor exhibited a significantly low LOD with good sensitivity, anti-interference ability, and stability. The authors stated that Tb-MOF sensors have the potential to detect nitrite ions in polluted water.

Hypochlorite (ClO^-) is an important disinfectant used for water purification. However, it should be properly monitored in drinking water because a high content of ClO^- may be dangerous to human health, whereas an inadequate amount will not kill microorganisms. Thus, in a recent study, an MOF-based fluorescent sensor (5-5-Eu/BPyDC@MOF-253-NH_2) was synthesized for the ratiometric detection of hypochlorite ClO^-.[227] The developed sensor exhibited the red emission of Eu and blue emission of the ligand. Upon the addition of ClO^-, it was observed that the emission at 417 nm was gradually suppressed, while that at 614 nm remained almost intact.[227] The sensor exhibited a response time of 15 s with a detection limit of 0.094 μm over a broad linear range of 0.1–30 μm. Further, it was used for the ratiometric on-off-on sensing of ascorbic acid. ClO^- was observed to decrease gradually upon the addition of ascorbic acid with the recovery of blue emission. The mechanism investigation suggested that a plausible mechanism for the observed quenching effect of the MOF-based sensor is based on the energy transfer between 5-5-Eu/BPyDC@MOF-253-NH_2 and ClO^-.[227]

5.1.4 Sensing of organic pollutants. Antibiotics and pesticides are another important class of organic water contaminants. They are very difficult to degrade in water and enter the food chain, posing a significant threat to human health. Therefore, monitoring and sensing of these species in water are important. Recently, a europium(III) MOF sensor with excellent luminescent properties was developed and used for the detection of a variety of antibiotics in water systems.[228] Liming Fan et al.[229] designed and developed a multi-response chemo-sensing platform based on Zn(II)-organic frameworks, $\{[Zn(tptc)_{0.5}(bimb)]\cdot H_2O\}_n$ (NUC-6), to determine pesticides and antibiotics in water. The chemical and thermal stability studies revealed that the developed system was fairly stable to be used as a luminescent sensor to detect contaminants in water. The developed platform was successfully used for the trace detection of 2,6-dichloro-4-nitroaniline (DCN) selectively in the presence

of other interfering pesticides. Its luminescence intensity was suppressed significantly in the presence of DCN. Further, the potential of the developed chemo-sensor was investigated for the selective detection of the antibiotics nitrofurazone (NFZ) and nitrofurantoin (NFT). As is evident from the luminescent results, NUC-6 could effectively detect NFZ and NFT with a detection limit of 12 ppm and 16 ppm, respectively. The spectroscopic investigations with quantum chemical calculations revealed that the inner filter effect (due to the strong absorption of the analyte at the excitation wavelength of the sensor) and photo-induced electron transfer are the plausible mechanisms for the luminescent quenching. In another report, Eu-BTB was prepared as a water-stable luminescent sensor for the selective detection of sulfamethazine antibiotics.[230] The fluorescence studies indicated that the "antenna effect" from the emission band of the ligand was not present in the Eu-MOF. The detection ability of the synthesized MoF sensor was studied using various antibiotics. Among them, SMZ displayed an excellent quenching of the fluorescent signal owing to the inner filter effect. Further, to investigate the application of the sensor probe in real samples, standard addition and recovery studies were performed on lake water samples. The percentage recovery of SMZ was observed to be in the range of 94–105.5%, indicating the practical applicability of the developed probe. The limit of detection for SMZ was observed to be 0.6555 μm over a broad linear range of 0–80 μm. Wang et al. developed 3D luminescent sensors for the determination of colchicine in the presence of interfering ions.[231] Besides the above-mentioned representative literature, there have been several other reports in recent years regarding the use of MOF-based luminescent sensors for the detection of a variety of water contaminants.[189–191,232–235]

5.2 MOF-based electrochemical sensors

In recent years, due to the porous structure, large surface area, and unique morphology of MOFs, metal–organic framework-based sensitive and selective electronic sensors have emerged as an advanced tool for sensing a variety of pollutants ranging from heavy metals to organic contaminants.[193–195,236–239]

An electrochemical sensor comprised of an aluminium-MOF was fabricated with excellent sensitivity for the detection of hydroquinone with excellent sensitivity.[240] In another report, a lanthanide-MOF was prepared for the detection of heavy metal ions.[241] The developed sensor exhibited high selectivity, sensitivity, and low detection limit for sensing Zn^{2+}, Cd^{2+}, Pb^{2+}, and Cu^{2+} ions. Also, a selective electrochemical sensor was developed using a combination of graphene aerogel (GA)–metal–organic framework (MOF) for the simultaneous detection of Cd^{2+}, Pd^{2+}, Cu^{2+} and Hg^{2+}.[242] The in situ growth of the MOF UiO-66-NH_2 crystal on the GA matrix was performed to synthesize the sensing material. Another sensor based on a graphene oxide/zinc-based metal–organic framework (GO/MOF) was fabricated to determine As^{3+} in water samples.[243] The sensor was prepared via a solvothermal method and modified on a glassy carbon electrode (GCE). The developed sensor showed an outstanding electrochemical performance in the linear working range of 0.2 to 25 ppb and a detection limit of 0.06 ppb.

The detection limit was even lower than the Environmental Protection Agency (EPA) value for As^{3+} in potable water.

In recent years, the ratiometric strategy has attracted attention to overcome the problem of reproducibility of electrochemical sensors. Recently, Wang *et al.* developed a highly accurate and reliable sensor based on the ratiometric strategy using a ferrocene carboxylic acid (Fc)-UiO-66-NH$_2$ MOF for the simultaneous detection of Cd^{2+}, Pb^{2+} and Cu^{2+} in aqueous medium.[244] The conductivity of the composite (trGNO/Fc-NH$_2$-UiO-66) was increased by introducing thermally reduced graphene oxide (trGNO). In addition, Fc significantly enhanced the conductance of the sensor. When applied in real tap water samples, peaks were not observed, indicating the absence of the studied ions in the tap water. Using the standard addition method, the recovery values for the detection of Cd^{2+}, Pb^{2+}, and Cu^{2+} were found to be 94.38–101.25%, 95.63–104.88%, and 90.63–94.38%, respectively.

4-Chloro-3-methyl phenol (PCMC) and 2,4-dichlorophenol (2,4-DCP) are among the chlorophenol pollutants that require urgent attention. The research group of Xumen Duan and Limen Lu utilized the conducting potential of poly(3,4-ethylenedioxy thiophene) (PEDOT) and large surface area of graphene aerogel (GA) to synthesize a novel MOF-based composite, UiO-66-NH$_2$@PEDOT/GA, as a high-performance electrochemical sensing platform for PCMC.[245] The modified electrode was prepared by combining UiO-66-NH$_2$@PEDOT/GA with a glassy carbon electrode (GCE). As evident from the electrochemical impedance spectroscopy investigations, there was a significant reduction in the electron transfer resistance (R_{ct}) value at UiO-66-NH$_2$@PEDOT/GCE after combining UiO-66-NH$_2$@PEDOT with GA. This suggests that an increase in the surface area and conductivity of the modified electrode owing to the synergistic effect of UiO-66-NH$_2$@PEDOT and GA. The electrochemical behavior of PCMC was investigated using the new electrode and it was observed that the electrochemical signal was significantly improved with UiO-66-NH$_2$@PEDOT/GA/GCE compared to the bare GCE and other combinations,[246] which may be attributed to the high conductivity and large surface area of UiO-66-NH$_2$@-PEDOT and 3D heterogeneous structure and efficient electron transfer paths of GA. Also, the experimental parameters including pH and accumulation time were optimized to obtain a sensitive sensor for PCMC. Under the optimized conditions, the sensitivity was observed to be 1.87 μA mM^{-1} cm^{-2} with a low detection limit of 0.2 μM. The developed sensing platform was found to be highly accurate, reproducible, reliable, and stable. Furthermore, the potential of the developed sensor was investigated to detect PCMC in tap water using the standard recovery method. The recovery results (93.2% to 106.4%) indicated the usability of the developed modified electrode in real samples. In another report, an electrochemical sensing electrode modifier based on copper benzene-1,3,5-tricarboxylate–graphene oxide (Cu-BTC/GO) was prepared *via* the solvothermal process for the selective detection of 2,4-dichlorophenol in aqueous solution.[247] Owing to the large surface area of Cu-BTC and the electrical properties of graphene, the number of reaction sites increased. Cyclic voltammetry, electrochemical impedance spectroscopy, and differential pulse voltammetry studies revealed that under

the optimized conditions, the developed sensor has a low detection limit (0.083 mM) in the range of 1.5–24 mM with high reproducibility and selectivity in the presence of interfering compounds. To demonstrate the practical application of the developed platform, it was used to detect 2,4-DCP in a lake water sample with satisfactory recovery. An electrochemical sensor comprised of iron(II) phthalocyanine (PcFe) and a zinc-based metal–organic framework was developed to detect and determine trichloroacetic acid,[248] which is considered a "Group 3" carcinogen by the International Agency for Research on Cancer.[249] The sensing was based on the reduction of PcFe(II) to PcFe(I), which is re-oxidized in the presence of trichloroacetic acid. Trichloroacetic acid was determined by measuring the reduction current of PcFe(II). The developed sensor was found to be extremely sensitive, selective, and stable.[250] A simple methodology was used to synthesize a sensing composite comprised of tetrakis(4-carboxyphenyl)porphyrin (TCPP) and Cu (CuTCPP) with platelet-ordered mesoporous carbon (pOMC). A modified electrode (CuTCPP/pOMC-3/GCE) was constructed using the developed sensor to detect hydroxylamine and chlorogenic acid. Combining pOMC with CuTCPP increased the conductivity. The sensor exhibited a broad linear range and low limit of detection for both analytes. The interfering ability of the developed sensor was investigated in the presence of a 100-fold concentration of a variety of ions and organic compounds. The results suggested that the developed CuTCPP/pOMC-3/GCE displayed superb anti-interfering ability. Moreover, the sensor was used to determine hydroxylamine and chlorogenic acid in real samples with satisfactory results.

The increasing use of antibiotics poses a serious threat to the environment and needs reliable sensing techniques. Thus, an electrode material based on a nanocomposite of Zr(IV) MOF, NH$_2$-UiO-66, and reduced graphene oxide (RGO) was designed and developed by the research group of Shun Mao for the trace detection of ciprofloxacin.[251] The sensing method used complexometric titration between ciprofloxacin and Cu^{2+}. The sensor exhibited a high electrochemical performance owing to its porosity, unique structure, large specific surface area, and high density of active sites. The developed platform (NH$_2$-UiO-66/RGO) showed a wide linear range from 0.02 to 1 μM with a sensitivity of 10.86 μA μM^{-1} to detect trace levels of ciprofloxacin (6.67 nM).

5.3 MOF-based colorimetric sensors

Colorimetric sensor-based techniques are considered extremely sensitive and quick to determine hazardous water contaminants. Using these sensors, detection is possible even with the naked eyes based on the color change.[252] Due to the specific interaction between organic ligands and metal ions, MOF-based colorimetric sensors have been proven to be reliable and accurate sensing platforms for the colorimetric detection of various water pollutants including heavy metal ions and organic pollutants. In an initial attempt, a Cu(I)-MOF colorimetric sensor comprised of Cu(I) and 1-benzimidazolyl-3,5-bis(4-pyridyl) benzene was designed for the naked-eye colorimetric detection of water and formaldehyde in very small quantities.[253] Wang *et al.*[254] designed

and synthesized an MOF-based porous nanocomposite of Fe_3O_4-decorated graphene (Fe_3O_4/rGO/MOF) for dual application in colorimetric detection and degradation of phenol in water systems. The hydrothermal method was used to prepare Fe_3O_4/rGO, and tannic acid was used to functionalize Fe_3O_4/rGO, which formed the sheet-like sandwich MOF composites. Using the developed composite, a colorimetric sensing platform comprised of Fe_3O_4/rGO/MOF, 4-amino antipyrine, and H_2O_2 was developed to detect phenol. Different concentrations of phenol were added to the system. The color of the solution gradually changed from pink to colorless. The system displayed a linear range of 10–80 μM with the limit of 3.33×10^{-6} M. The results demonstrated that the developed composite displayed enzyme mimic properties, which were used to detect phenol in water solution by visual inspection. Moreover, the developed MOF-based system was successfully used as a Fenton-like catalyst to degrade phenol. In another study, the synthesis of a 2D-bimetallic Co/Mn-MOF with sheet-like morphology was reported through a simple hydrothermal method.[255] The developed material was used as a colorimetric sensor to determine H_2O_2 via peroxidase-like activity. Under the optimized conditions, the sensing probe displayed a linear absorbance range in the concentration range of 1 to 100 μM with a detection limit of 0.85 μM. Further, the practical application of the sensor was investigated in real samples with good recovery. Jinlou Gu and co-workers fabricated a sensitive Ru-based MOF (RuUiO-67MOF) nanocomposite to selectively detect mercury ions.[256] The authors reported that Ru was trapped in the MOF framework and acted as an active site and signal detector. The developed sensing platform was found to change color from red to yellow after the addition of mercury ions, which could be easily observed even with the naked eye. The UV-visible spectroscopy results revealed that the intensity of the absorption band observed at 540 decreased gradually on increasing the concentration of Hg ions, while that of the absorption band at 435 nm increased.[256] Hg^{2+} could be detected at a concentration as low as 0.5 μM. The interference study confirmed the selectivity of the probe in the presence of major interfering cations. Further, the sensor could be easily regenerated with the addition of KI solution.

5.4 MOF-based SERS sensors

Surface-enhanced Raman scattering (SERS) is a versatile, rapid, non-destructive, and highly sensitive analytical technique used to detect a variety of analytes ranging from chemicals to biomolecules. The analyte molecules are mixed with a colloidal solution or adsorbed on the roughened surface of a metal, which leads to an enhancement in the Raman signals by several-fold. The SERS substrate plays a key role in achieving promising detection results using the SERS technique. The enhancement may be either electromagnetic through metal atoms (Ag and Au) or chemical through various composite substrates. In recent years, MOF-based materials have attracted tremendous interest from researchers in SERS detection owing to their unique porous structure, large surface area, and superb stability.[257] Initially, Yu et al. observed the SERS effect on an MOF surface.[258] Since then, several MOF-based SERS substrates

have been developed to detect water contaminants[259] including dyes[260] and organic pollutants.[261,262] Jing Wang and coworkers developed composites of MOFs (MOF-199) with gold nanoparticles for SERS detection.[263] The developed substrate was used successfully to detect pesticides with a good detection limit. A highly sensitive and stable SERS active substrate was developed by embedding gold nanoparticles in the host matrix of an MOF, MIL-1-1.[260] The developed substrate exhibited a significant SERS enhancement when used with different analytes. The authors stated that the synergistic effect of the localized surface plasmon resonance (LSPR) of the Au nanoparticles and the adsorption efficiency of the MOF were responsible for the remarkable SERS activity. The practical applicability of the developed SERS sensing substrate was investigated for the quantification of p-phenylenediamine, an organic pollutant in environmental water, and alpha-fetoprotein, a tumor marker in human serum. In the case of p-phenylenediamine, the linearity range was observed to be 1.0–100.0 ng mL^{-1}, while that for alpha-fetoprotein was 1.0–130.0 ng mL^{-1}. Furthermore, good recoveries were obtained for both p-phenylenediamine (80.5% to 114.7%) and alpha-fetoprotein (79.3% to 107.3%). A core–shell nanocomposite (MOF, HKUST-1 (Cu)@Ag nanoparticles) was electrodeposited on a screen-printed carbon electrode as a sensitive and reliable SERS substrate for the selective detection of polycyclic aromatic hydrocarbons.[264] The combined effect of the large number of "hotspots" due to the Ag NPs and the good adsorption power of the MOF resulted in an enhancement in the SERS signals. The optimized SERS probe could effectively detect 4-amino thiophenol even at a very low concentration (5×10^{-10} M). This method was reported to detect a wide range of PAH concentrations (0.5 nM to 0.5 M) with low detection limits (hundreds of pM). Fugang Xu et al. designed an MOF-based core–shell nanohybrid comprised of magnetic Fe_3O_4 as the core and Au NP interlayer-MIL-100(Fe) as the shell with the formula Fe_3O_4-Au@MIL-100(Fe).[265] The magnetic core not only produced a reproducible and enhanced SERS signal but also enabled rapid separation and concentration. The signal was further enhanced due to the chemical enhancement effect of the MOF shell. The developed multifunctional SERS substrate was successfully used for the quantification of malachite green (dye) and thiram (pesticide) in a standard sample and lake water sample. The detection limit for MG was reported to be as low as 10^{-8} M and that of thiram was observed as 10^{-7} M. Further, the substrate could be easily recycled via ultra-sonication for several cycles. In a recent study, Wei Song et al. reported the fabrication of a multifunctional MOF-based nanocomposite for the sensitive SERS detection of cationic dyes.[266] The developed substrate acted as a peroxidase-like enzyme to degrade cationic dyes. Another peroxidase-like MOF-based magnetic SERS sensor with the composition of Ni@Mil-100(Fe)@Ag nanowires was developed for the determination of various cationic dyes.[267] The SERS probe based on nickel nanowires could detect and remove the contaminant very rapidly without any tedious pre-concentration processes. The limit of detection was observed to be 10^{-10} M for crystal violet. Moreover, the substrate was easily recyclable. As is evident from the literature, although researchers are

continuously investigating the potential of MOFs for the sensitive SERS detection of analytes, still there are some challenges such as investigating the detailed enhancement mechanism and developing more sensitive MOF-based SERS substrates with better stability and selectivity, which should be addressed to widen their practical applications.

6. Challenges and future prospects

There are various challenges in the development of MOFs for commercial applications. In the field of adsorption, MOFs tend to have relatively low selectivity, *i.e.*, they adsorb a variety of different compounds, including both desirable and undesirable compounds. This makes it difficult to use MOFs for the targeted adsorption of specific water contaminants. Also, MOFs typically have low loading capacities, where they can only absorb a limited amount of a particular contaminant before becoming saturated. This limits their effectiveness for large-scale applications. Moreover, MOFs are usually more expensive than other types of adsorbents, such as activated carbon and zeolites, making them less attractive for commercial applications. In addition, MOFs are also prone to deactivation, *i.e.*, they can lose their adsorptive properties over time. This can lead to decreased efficiency and increased costs.

For photocatalytic applications, MOFs have low thermal and chemical stability due to their porous structure and organic linkers. Consequently, they are not suitable for the long-term photocatalytic degradation of water contaminants. MOFs typically have lower surface area than other materials such as titanium oxide, making them less efficient in photocatalytic degradation processes. Also, the light absorption by many MOFs due to their weak conjugation and lack of specific functional groups is another factor limiting their application. Generally, MOFs are expensive due to their complex synthetic methods, and they exhibit low activity. Regarding their sensing applications, MOFs are not as sensitive to water contaminants as traditional sensors such as spectral sensors. MOFs are more expensive than traditional sensing methods, which makes them prohibitively expensive for monitoring water contaminants on a large scale. Also, MOFs are more prone to degradation due to their sensitivity to moisture and humidity, which can reduce their sensitivity and accuracy. MOFs are not always selective in their sensing capabilities, and thus they may detect other compounds besides water contaminants. Also, MOFs are difficult to fabricate due to their complexity and the need for precise control of the synthesis conditions.

The performance and properties of MOFs can be improved by careful selection of organic ligands with specific functional groups and metal ions. The synthesis conditions such as solvent, temperature, time, and pressure need to be adjusted cautiously to impart specific properties in MOFs. New properties and enhanced stability can be introduced in MOFs by post-synthetic modifications. Water stability is crucial for applications in aqueous environments. The selection of metal nodes and organic linkers that are stable in water and can form robust coordination bonds and the consideration of using metal nodes with high oxidation states, which result in stronger metal–ligand bonds, are

the two primary approaches for the fabrication of water-stable MOFs. Hydrophobic groups or groups that can coordinate with water molecules in a controlled manner may improve their stability. This can also be achieved by incorporating hydrophobic ligands or introducing hydrophobic coatings. Understanding the environmental conditions and performance expectations is crucial for optimizing water stability of MOFs and their widespread application for water remediation.

Despite their many limitations, MOFs have emerged as promising materials for water remediation applications due to their unique properties such as large surface area, high porosity, and tunable composition. MOFs have been extensively studied for water purification, capture of pollutants, and heavy metal removal. MOFs are also being explored for the removal of organic pollutants and antibiotics. In the future, MOFs can be used to create more efficient, cost-effective, and environmentally friendly water remediation systems. Additionally, MOFs can be used to create systems that are more selective and efficient at removing specific types of contaminants. Furthermore, MOFs can also be used to create systems that can be tailored to a specific application, such as the removal of specific types of pollutants or heavy metals. Overall, MOFs have tremendous potential for water remediation applications and can revolutionize the way we clean and purify water.

7. Conclusion

MOFs have been recently used as adsorbents for the removal of a wide range of water contaminants, such as heavy metal ions, organic pollutants, dyes, and pharmaceuticals. The adsorption capacity of MOFs is higher than that of other adsorbents due to their large surface area, high porosity, and tunable pore size. In addition to their adsorption properties, MOFs can be used for the photocatalytic degradation of water contaminants. Photocatalysis is a powerful technique that can be used to degrade a wide range of water contaminants. MOFs have been used for the photocatalytic degradation of organic pollutants, such as dyes, and pharmaceuticals. MOFs have also been developed as emerging sensors for environmental contaminants. MOFs are effective at detecting and quantifying target molecules, even at very low concentrations, due to their high porosity and large surface area. MOFs can be tailored to target specific molecules and used in conjunction with other sensing techniques such as fluorescence and electrochemical detection. Thus, MOFs offer a novel approach for the removal and degradation of water contaminants, and further research is needed to exploit their full potential. Accordingly, the application of MOFs is expected to expand in the coming years.

Conflicts of interest

There are no conflicts to declare.

Acknowledgements

References

1 L. Lin, H. Yang and X. Xu, *Front. Environ. Sci.*, 2022, **10**, 880246.

2 X. Xu, H. Yang and C. Li, *Int. J. Environ. Res. Public Health*, 2022, **19**, 3532.

3 A. Saravanan, P. Senthil Kumar, S. Jeevanantham, S. Karishma, B. Tajsabreen, P. R. Yaashikaa and B. Reshma, *Chemosphere*, 2021, **280**, 130595.

4 H. Li, M. Eddaoudi, M. O'Keeffe and O. M. Yaghi, *Nature*, 1999, **402**, 276–279.

5 S. Mukherjee, S. Dutta, Y. D. More, S. Fajal and S. K. Ghosh, *Dalton Trans.*, 2021, **50**, 17832–17850.

6 J. Fonseca, T. Gong, L. Jiao and H. L. Jiang, *J. Mater. Chem. A*, 2021, **9**, 10562–10611.

7 Y. Zhang, Y. Zhou, Y. Zhao and C. J. Liu, *Catal. Today*, 2016, **263**, 61–68.

8 D. Yang and B. C. Gates, *ACS Catal.*, 2019, **9**, 1779–1798.

9 M. Bilal, M. Adeel, T. Rasheed and H. M. N. Iqbal, *J. Mater. Res. Technol.*, 2019, **8**, 2359–2371.

10 P. Kumar, A. Deep and K. H. Kim, *TrAC, Trends Anal. Chem.*, 2015, **73**, 39–53.

11 Z. Zhang, Y. Zhao, Q. Gong, Z. Lib and J. Li, *Chem. Commun.*, 2013, **49**, 653–661.

12 C. Y. Lee, O. K. Farha, B. J. Hong, A. A. Sarjeant, S. T. Nguyen and J. T. Hupp, *J. Am. Chem. Soc.*, 2011, **133**, 15858–15861.

13 S. M. F. Vilela, T. Devic, A. Várez, F. Salles and P. Horcajada, *Dalton Trans.*, 2019, **48**, 11181–11185.

14 X. Zhao, Y. Wang, D. S. Li, X. Bu and P. Feng, *Adv. Mater.*, 2018, **30**, 1705189.

15 S. Rojas, A. Arenas-Vivo and P. Horcajada, *Coord. Chem. Rev.*, 2019, 388.

16 S. Rojas and P. Horcajada, *Chem. Rev.*, 2020, 120.

17 N. C. Burtch, H. Jasuja and K. S. Walton, *Chem. Rev.*, 2014, 114.

18 Z. Wu, X. Yuan, H. Zhong, H. Wang, L. Jiang, G. Zeng, H. Wang, Z. Liu and Y. Li, *J. Mol. Liq.*, 2017, **247**, 215–229.

19 H. Kaur, N. Devi, S. S. Siwal, W. F. Alsanie, M. K. Thakur and V. K. Thakur, *ACS Omega*, 2023, 8.

20 J. Xia, Y. Gao and G. Yu, *J. Colloid Interface Sci.*, 2021, **590**, 495–505.

21 X. Fang, B. Zong and S. Mao, *Nano-Micro Lett.*, 2018, **10**, 64.

22 S. Dutta, S. Let, S. Sharma, D. Mahato and S. K. Ghosh, *Chem. Rec.*, 2021, 21.

23 H. Bunzen, *ChemNanoMat*, 2021, **7**, 998–1007.

24 F. Rouhani and A. Morsali, *Chem.—Eur. J.*, 2018, **24**, 17170–17179.

25 H. Konnerth, B. M. Matsagar, S. S. Chen, M. H. G. Prechtl, F. K. Shieh and K. C. W. Wu, *Coord. Chem. Rev.*, 2020, **416**, 213319.

26 M. J. Zaworotko, *Nat. Chem.*, 2009, **1**, 267–268.

27 Z. Li, L. Wang, L. Qin, C. Lai, Z. Wang, M. Zhou, L. Xiao, S. Liu and M. Zhang, *Chemosphere*, 2021, **285**, 131432.

28 S. Sharma, S. Dutta, G. K. Dam and S. K. Ghosh, *Chem.– Asian J.*, 2021, 16.

29 C. Wang, X. Liu, N. K. Demir, J. P. Chen and K. Li, *Chem. Soc. Rev.*, 2016, **45**, 5107–5134.

30 B. Liu, K. Vikrant, K. H. Kim, V. Kumar and S. K. Kailasa, *Environ. Sci.: Nano*, 2020, **7**, 1319–1347.

31 H. Jasuja, Y. Jiao, N. C. Burtch, Y.-G. Huang and K. S. Walton, *Langmuir*, 2014, **30**(47), 14300–14307.

32 J. Zhang, P. Li, X. Zhang, X. Ma and B. Wang, *ACS Appl. Mater. Interfaces*, 2020, **12**, 46057–46064.

33 K. Zu, M. Qin and S. Cui, *Renewable Sustainable Energy Rev.*, 2020, **133**, 110246.

34 Z. Yu, X. Cao, S. Wang, H. Cui, C. Li and G. Zhu, *Water, Air, Soil Pollut.*, 2021, **232**, 1–19.

35 M. Ding, X. Cai and H.-L. Jiang, *Chem. Sci.*, 2019, **10**, 10209–10230.

36 N. Li, J. Xu, R. Feng, T.-L. Hu and X.-H. Bu, *Chem. Commun.*, 2016, **52**, 8501–8513.

37 A. E. Baumann, D. A. Burns, B. Liu and V. S. Thoi, *Commun. Chem.*, 2019, **2**, 86.

38 L. Feng, K.-Y. Wang, G. S. Day, M. R. Ryder and H.-C. Zhou, *Chem. Rev.*, 2020, **120**, 13087–13133.

39 X. Shen, K. Hii Ru Yie, X. Wu, Z. Zhou, A. Sun, A. M. Al- bishari, K. Fang, M. A. Al- Baadani, Z. Deng, P. Ma and J. Liu, *Chem. Eng. J.*, 2022, **430**, 133094.

40 Y. Liang, W. Hu, X. Yuan, Z. Zeng, B. Zhu and Y. Gu, *Adv. Opt. Mater.*, 2022, **10**, 2200779.

41 X. Zhang, B. Wang, A. Alsalme, S. Xiang, Z. Zhang and B. Chen, *Coord. Chem. Rev.*, 2020, **423**, 213507.

42 L. Wang, X. Li, B. Yang, K. Xiao, H. Duan and H. Zhao, *Chem. Eng. J.*, 2022, **450**, 138215.

43 X. Zhang, Y. Liu, L. Kong, H. Liu, J. Qiu, W. Han, L.-T. Weng, K. L. Yeung and W. Zhu, *J. Mater. Chem. A*, 2013, **1**, 10635–10638.

44 L. H. Xie, M. M. Xu, X. M. Liu, M. J. Zhao and J. R. Li, *Advanced Science*, 2020, **7**, 1901758.

45 V. Guillerm, F. Ragon, M. Dan-Hardi, T. Devic, M. Vishnuvarthan, B. Campo, A. Vimont, G. Clet, Q. Yang, G. Maurin, G. Férey, A. Vittadini, S. Gross and C. Serre, *Angew. Chem., Int. Ed.*, 2012, **51**, 9267–9271.

46 T. Wu, L. Shen, M. Luebbers, C. Hu, Q. Chen, Z. Ni and R. I. Masel, *Chem. Commun.*, 2010, **46**, 6120–6122.

47 K. K. Tanabe and S. M. Cohen, *Chem. Soc. Rev.*, 2011, **40**, 498–519.

48 J. Aguilera-Sigalat and D. Bradshaw, *Chem. Commun.*, 2014, **50**, 4711–4713.

49 T. Islamoglu, S. Goswami, Z. Li, A. J. Howarth, O. K. Farha and J. T. Hupp, *Acc. Chem. Res.*, 2017, **50**, 805–813.

50 S. A. Tirmizi, A. Badshah, H. M. Ammad, M. Jawad, S. M. Abbas, U. A. Rana and S. U.-D. Khan, *Arabian J. Chem.*, 2018, **11**, 26–33.

51 D. Meili and J. Hai-Long, *CCS Chem.*, 2020, **3**, 2740–2748.

52 L. H. Mohd Azmi, P. Cherukupally, E. Hunter-Sellars, B. P. Ladewig and D. R. Williams, *Chem. Eng. J.*, 2022, **429**, 132304.

53 X. Liu, Y. Li, Y. Ban, Y. Peng, H. Jin, H. Bux, L. Xu, J. Caro and W. Yang, *Chem. Commun.*, 2013, **49**, 9140–9142.

54 D.-D. Zu, L. Lu, X.-Q. Liu, D.-Y. Zhang and L.-B. Sun, *J. Phys. Chem. C*, 2014, **118**, 19910–19917.

55 S. Dutta, Y. D. More, S. Fajal, W. Mandal, G. K. Dam and S. K. Ghosh, *Chem. Commun.*, 2022, **58**, 13676–13698.

56 A. Karmakar, A. V Desai and S. K. Ghosh, *Coord. Chem. Rev.*, 2016, **307**, 313–341.

57 S. N. Zhao, Y. Zhang, S. Y. Song and H. J. Zhang, *Coord. Chem. Rev.*, 2019, 398.

58 P. Kumar, A. Pournara, K.-H. Kim, V. Bansal, S. Rapti and M. J. Manos, *Prog. Mater. Sci.*, 2017, **86**, 25–74.

59 H. He, L. Hashemi, M. L. Hu and A. Morsali, *Coord. Chem. Rev.*, 2018, 376.

60 A. B. Spore and N. L. Rosi, *CrystEngComm*, 2017, **19**, 5417–5421.

61 Y.-X. Tan, Y.-P. He and J. Zhang, *Chem. Mater.*, 2012, **24**, 4711–4716.

62 D. F. Sava, V. Ch. Kravtsov, F. Nouar, L. Wojtas, J. F. Eubank and M. Eddaoudi, *J. Am. Chem. Soc.*, 2008, **130**, 3768–3770.

63 F. Nouar, J. Eckert, J. F. Eubank, P. Forster and M. Eddaoudi, *J. Am. Chem. Soc.*, 2009, **131**, 2864–2870.

64 S. Hasegawa, S. Horike, R. Matsuda, S. Furukawa, K. Mochizuki, Y. Kinoshita and S. Kitagawa, *J. Am. Chem. Soc.*, 2007, **129**, 2607–2614.

65 R. Ameloot, M. Aubrey, B. M. Wiers, A. P. Gómora-Figueroa, S. N. Patel, N. P. Balsara and J. R. Long, *Chem.–Eur. J.*, 2013, **19**, 5533–5536.

66 Z. Luo, S. Fan, J. Liu, W. Liu, X. Shen, C. Wu, Y. Huang, G. Huang, H. Huang and M. Zheng, *Polymers*, 2018, **10**(2), 209.

67 Z. Hasan and S. H. Jhung, *J. Hazard. Mater.*, 2015, **283**, 329–339.

68 E. M. Dias and C. Petit, *J. Mater. Chem. A*, 2015, **3**, 22484–22506.

69 L. Huang, R. Shen and Q. Shuai, *J. Environ. Manage.*, 2021, **277**, 111389.

70 N. A. A. Qasem, R. H. Mohammed and D. U. Lawal, *npj Clean Water*, 2021, **4**, 36.

71 L. Joseph, B.-M. Jun, M. Jang, C. M. Park, J. C. Muñoz-Senmache, A. J. Hernández-Maldonado, A. Heyden, M. Yu and Y. Yoon, *Chem. Eng. J.*, 2019, **369**, 928–946.

72 V. Russo, M. Hmoudah, F. Broccoli, M. R. Iesce, O.-S. Jung and M. Di Serio, *Front. Chem. React. Eng.*, 2020, **2**, 581487.

73 V. K. M. Au, *Front. Chem.*, 2020, **8**, 1–7.

74 A. A. Mohammadi, A. Alinejad, B. Kamarehie, S. Javan, A. Ghaderpoury, M. Ahmadpour and M. Ghaderpoori, *Int. J. Environ. Sci. Technol.*, 2017, **14**, 1959–1968.

75 D. D. C. Básicas, U. Autónoma, M. Azcapotzlaco, A. San, C. R. Tamaulipas and C. De, *México*, 2016, **3**, 331–334.

76 M. Dadashi Firouzjaei, F. Akbari Afkhami, M. Rabbani Esfahani, C. H. Turner and S. Nejati, *J. Water Process. Eng.*, 2020, **34**, 101180.

77 X. Xie, X. Huang, W. Lin, W. Lin, Y. Chen, X. Lang, Y. Wang, L. Gao, H. Zhu and J. Chen, *ACS Omega*, 2020, **5**, 13595–13600.

78 K. Iman, M. Shahid, M. S. Khan, M. Ahmad and F. Sama, *CrystEngComm*, 2019, **21**, 5299–5309.

79 Y. Y. Jia, G. J. Ren, A. L. Li, L. Z. Zhang, R. Feng, Y. H. Zhang and X. H. Bu, *Cryst. Growth Des.*, 2016, **16**, 5593–5597.

80 S. Lin, Z. Song, G. Che, A. Ren, P. Li, C. Liu and J. Zhang, *Microporous Mesoporous Mater.*, 2014, **193**, 27–34.

81 M. Samal, J. Panda, B. P. Biswal and R. Sahu, *CrystEngComm*, 2018, **20**, 2486–2490.

82 K. Karami, S. M. Beram, P. Bayat, F. Siadatnasab and A. Ramezanpour, *J. Mol. Struct.*, 2022, **1247**, 131352.

83 V. Javanbakht and Z. Rafiee, *J. Mol. Struct.*, 2022, **1249**, 131552.

84 X. Xue, Y. Weng, S. Yang, S. Meng, Z. Zhang, G. Yi and Y. Zhang, *Environ. Sci. Pollut. Res.*, 2021, **28**, 15883–15889.

85 X. X. Huang, L. G. Qiu, W. Zhang, Y. P. Yuan, X. Jiang, A. J. Xie, Y. H. Shen and J. F. Zhu, *CrystEngComm*, 2012, **14**, 1613–1617.

86 M. Kasula, T. Le, A. Thomsen and M. Rabbani Esfahani, *Chem. Eng. J.*, 2022, **439**, 135542.

87 S. H. Ghoochani, A. Heshmati, H. A. Hosseini and M. Darroudi, *Environ. Sci. Pollut. Res.*, 2022, **29**, 34406–34418.

88 E. R. García, R. L. Medina, M. M. Lozano, I. Hernández Pérez, M. J. Valero and A. M. M. Franco, *Materials*, 2014, **7**, 8037–8057.

89 Z. Zhang, J. Zhang, J. Liu, Z. Xiong and X. Chen, *Water, Air, Soil Pollut.*, 2016, **227**, 471.

90 S.-C. Wu, X. You, C. Yang and J.-H. Cheng, *Water Sci. Technol.*, 2017, **75**(12), 2800–2810.

91 L. Yang, Y.-L. Liu, C.-G. Liu, Y. Fu and F. Ye, *J. Mol. Liq.*, 2020, **300**, 112311.

92 H. Y. Chi, S. H. Hung, M. Y. Kan, L. W. Lee, C. H. Lam, J. J. Chen and D. Y. Kang, *CrystEngComm*, 2018, **20**, 5465–5474.

93 M. Z. Wu, J. Y. Shi, P. Y. Chen, L. Tian and J. Chen, *Inorg. Chem.*, 2019, **58**, 3130–3136.

94 R. S. Salama, E. S. M. El-Sayed, S. M. El-Bahy and F. S. Awad, *Colloids Surf., A*, 2021, **626**, 127089.

95 H. C. Woo and S. H. Jhung, *Chem. Eng. J.*, 2021, **425**, 130598.

96 M. Hasanzadeh, A. Simchi and H. Shahriyari Far, *J. Ind. Eng. Chem.*, 2020, **81**, 405–414.

97 S. M. Hassan, A. A. Ibrahim and D. A. Mohamed, *Int. J. Mod. Chem.*, 2017, **2017**, 111–126.

98 C. I. Ezugwu, Md. A. Asraf, X. Li, S. Liu, C.-M. Kao, S. Zhuiykov and F. Verpoort, *Data Brief*, 2018, **18**, 1952–1961.

99 W. Li, X. Du and H. He, *Research and Application of Materials Science*, 2019, **1**, 39–44.

100 S. Kim, J. Lee, Y. Son and M. Yoon, *Bull. Korean Chem. Soc.*, 2020, **41**, 843–850.

101 K. Liu, L. Deng, H. Li, Y. Bao, Z. Xiao, B. Li, Q. Zhou, Y. Geng and L. Wang, *J. Solid State Chem.*, 2019, **275**, 1–7.

102 C. Zhang, H. Li, C. Li and Z. Li, *Molecules*, 2020, **25**(1), 168.

103 H. Xue, X. S. Huang, Q. Yin, X. J. Hu, H. Q. Zheng, G. Huang and T. F. Liu, *Cryst. Growth Des.*, 2020, **20**, 4861–4866.

104 J. M. Yang, R. J. Ying, C. X. Han, Q. T. Hu, H. M. Xu, J. H. Li, Q. Wang and W. Zhang, *Dalton Trans.*, 2018, **47**, 3913–3920.

105 M. del Rio, J. C. Grimalt Escarabajal, G. Turnes Palomino and C. Palomino Cabello, *Chem. Eng. J.*, 2022, **428**, 131147.

106 K. Ahmad, H. U. R. Shah, S. Parveen, T. Aziz, H. A. Naseem, M. Ashfaq and A. Rauf, *J. Mol. Struct.*, 2021, **1242**, 130898.

107 N. Hassan, A. Shahat, I. M. El-Deen, M. A. M. El-Afify and M. A. El-Bindary, *J. Mol. Struct.*, 2022, **1258**, 132662.

108 F. Zadehahmadi, N. T. Eden, H. Mahdavi, K. Konstas, J. I. Mardel, M. Shaibani, P. C. Banerjee and M. R. Hill, *Environ. Sci.*, 2023, **9**, 1305–1330.

109 H. Shayegan, G. A. M. Ali and V. Safarifard, *ChemistrySelect*, 2020, **5**, 124–146.

110 Y. Chen, X. Bai and Z. Ye, *Nanomaterials*, 2020, **10**, 1–23.

111 D. T. Sun, L. Peng, W. S. Reeder, S. M. Moosavi, D. Tiana, D. K. Britt, E. Oveisi and W. L. Queen, *ACS Cent. Sci.*, 2018, **4**, 349–356.

112 J. Hou, H. Wang and H. Zhang, *Ind. Eng. Chem. Res.*, 2020, **59**, 12907–12923.

113 F. Ahmadijokani, S. Tajahmadi, A. Bahi, H. Molavi, M. Rezakazemi, F. Ko, T. M. Aminabhavi and M. Arjmand, *Chemosphere*, 2021, **264**, 128466.

114 M. Lu, L. Li, S. Shen, D. Chen and W. Han, *New J. Chem.*, 2019, **43**, 1032–1037.

115 S. Jamshidifard, S. Koushkbaghi, S. Hosseini, S. Rezaei, A. Karamipour, A. Jafari rad and M. Irani, *J. Hazard. Mater.*, 2019, **368**, 10–20.

116 A. Abbasi, T. Moradpour and K. Van Hecke, *Inorg. Chim. Acta*, 2015, **430**, 261–267.

117 J. M. Rivera, S. Rincón, C. Ben Youssef and A. Zepeda, *J. Nanomater.*, 2016, 8095737.

118 H. Zakeri, *Asian J. Chem.*, 2017, **29**, 1757–1760.

119 J. E. Efome, D. Rana, T. Matsuura and C. Q. Lan, *ACS Appl. Mater. Interfaces*, 2018, **10**, 18619–18629.

120 H. Xue, Q. Chen, F. Jiang, D. Yuan, G. Lv, L. Liang, L. Liu and M. Hong, *Chem. Sci.*, 2016, **7**, 5983–5988.

121 A. S. Yusuff, L. T. Popoola and E. O. Babatunde, *Appl. Water Sci.*, 2019, **9**, 1–11.

122 F. Rouhani, F. Rafizadeh-Masuleh and A. Morsali, *J. Am. Chem. Soc.*, 2019, **141**, 11173–11182.

123 A. A. Alqadami, M. Naushad, Z. A. Alothman and A. A. Ghfar, *ACS Appl. Mater. Interfaces*, 2017, **9**, 36026–36037.

124 F. Liu, S. Song, G. Cheng, W. Xiong, L. Shi and Y. Zhang, *Adsorpt. Sci. Technol.*, 2018, **36**, 1550–1567.

125 F. Yu, Y. Chen, Y. Wang, C. Liu and J. Qin, *J. Mater. Res.*, 2020, **35**, 299–311.

126 X. Hou, H. Zhou, J. Zhang, Y. Cai, F. Huang and Q. Wei, *Part. Part. Syst. Charact.*, 2018, **35**, 1700438.

127 X. Xiao, Y. Deng, J. Xue and Y. Gao, *Environ. Technol.*, 2021, **42**, 1930–1942.

128 L. Esrafili, V. Safarifard, E. Tahmasebi, M. D. Esrafili and A. Morsali, *New J. Chem.*, 2018, **42**, 8864–8873.

129 Y. Peng, H. Huang, Y. Zhang, C. Kang, S. Chen, L. Song, D. Liu and C. Zhong, *Nat. Commun.*, 2018, **9**, 187.

130 L. Zhao, M. R. Azhar, X. Li, X. Duan, H. Sun, S. Wang and X. Fang, *J. Colloid Interface Sci.*, 2019, **542**, 421–428.

131 A. V. Desai, B. Manna, A. Karmakar, A. Sahu and S. K. Ghosh, *Angew. Chem.*, 2016, **128**, 7942–7946.

132 A. V. Desai, B. Manna, A. Karmakar, A. Sahu and S. K. Ghosh, *Angew. Chem., Int. Ed.*, 2016, **128**(27), 7942–7946.

133 S. Dutta, P. Samanta, B. Joarder, S. Let, D. Mahato, R. Babarao and S. K. Ghosh, *ACS Appl. Mater. Interfaces*, 2020, **12**, 41810–41818.

134 S. Sharma, S. Let, A. V. Desai, S. Dutta, G. Karuppasamy, M. M. Shirolkar, R. Babarao and S. K. Ghosh, *J. Mater. Chem. A*, 2021, **9**, 6499–6507.

135 J. Li, Y. N. Wu, Z. Li, B. Zhang, M. Zhu, X. Hu, Y. Zhang and F. Li, *J. Phys. Chem. C*, 2014, **118**, 27382–27387.

136 T. A. Vu, G. H. Le, C. D. Dao, L. Q. Dang, K. T. Nguyen, Q. K. Nguyen, P. T. Dang, H. T. K. Tran, Q. T. Duong, T. V. Nguyen and G. D. Lee, *RSC Adv.*, 2015, **5**, 5261–5268.

137 C. Wang, X. Liu, J. P. Chen and K. Li, *Sci. Rep.*, 2015, **5**, 1–10.

138 B. Liu, M. Jian, R. Liu, J. Yao and X. Zhang, *Colloids Surf., A*, 2015, **481**, 358–366.

139 M. Jian, H. Wang, R. Liu, J. Qu, H. Wang and X. Zhang, *Environ. Sci.: Nano*, 2016, **3**, 1186–1194.

140 J. Li, Y. Liu, Y. Ai, A. Alsaedi, T. Hayat and X. Wang, *Chem. Eng. J.*, 2018, **354**, 790–801.

141 L. Esrafili, M. Gharib and A. Morsali, *Dalton Trans.*, 2019, **48**, 17831–17839.

142 R. Ricco, K. Konstas, M. J. Styles, J. J. Richardson, R. Babarao, K. Suzuki, P. Scopece and P. Falcaro, *J. Mater. Chem. A*, 2015, **3**, 19822–19831.

143 L. Fu, S. Wang, G. Lin, L. Zhang, Q. Liu, H. Zhou, C. Kang, S. Wan, H. Li and S. Wen, *J. Cleaner Prod.*, 2019, **229**, 470–479.

144 K. Wang, J. Gu and N. Yin, *Ind. Eng. Chem. Res.*, 2017, **56**, 1880–1887.

145 F. H. M. Tang, M. Lenzen, A. McBratney and F. Maggi, *Nat. Geosci.*, 2021, **14**, 206–210.

146 M. A. Hassaan and A. El Nemr, *Egypt. J. Aquat. Res.*, 2020, **46**, 207–220.

147 G. Liu, L. Li, D. Xu, X. Huang, X. Xu, S. Zheng, Y. Zhang and H. Lin, *Carbohydr. Polym.*, 2017, **175**, 584–591.

148 X. Wang, X. Ma, H. Wang, P. Huang, X. Du and X. Lu, *Microchim. Acta*, 2017, **184**, 3681–3687.

149 E. Abdelillah Ali Elhussein, S. Şahin and Ş. S. Bayazit, *J. Mol. Liq.*, 2018, **255**, 10–17.

150 G. Liu, L. Li, X. Huang, S. Zheng, X. Xu, Z. Liu, Y. Zhang, J. Wang, H. Lin and D. Xu, *J. Mater. Sci.*, 2018, **53**, 10772–10783.

151 O. Semyonov, S. Chaemchuen, A. Ivanov, F. Verpoort, Z. Kolska, M. Syrtanov, V. Svorcik, M. S. Yusubov, O. Lyutakov, O. Guselnikova and P. S. Postnikov, *Appl. Mater. Today*, 2021, **22**, 100910.

152 P. Kumar, P. Kumar, A. Deep and L. M. Bharadwaj, *Adv. Mater. Res.*, 2012, **488–489**, 1543–1546.

153 T. Li, M. Lu, Y. Gao, X. Huang, G. Liu and D. Xu, *J. Adv. Res.*, 2020, **24**, 159–166.

154 N. I. F. Aris, N. A. Rahman, M. H. Wahid, N. Yahaya, A. S. A. Keyon and S. Kamaruzaman, *R. Soc. Open Sci.*, 2020, **7**, 192050.

155 Q. Xie, Y. Li, Z. Lv, H. Zhou, X. Yang, J. Chen and H. Guo, *Sci. Rep.*, 2017, **7**, 1–15.

156 Q. Yang, J. Wang, W. Zhang, F. Liu, X. Yue, Y. Liu, M. Yang, Z. Li and J. Wang, *Chem. Eng. J.*, 2017, **313**, 19–26.

157 J. Pot E, M. Milakovic, A. Chaumot, S. Seidensticker, M. Melling, A. Supriatin and S. Sherif, *Proc. Natl. Acad. Sci. U. S. A.*, 2022, **119**(8), e2113947119.

158 M. Ortúzar, M. Esterhuizen, D. R. Olicón-Hernández, J. González-López and E. Aranda, *Front. Microbiol.*, 2022, **13**, 869332.

159 Z. Luo, H. Chen, S. Wu, C. Yang and J. Cheng, *Chemosphere*, 2019, **237**, 124493.

160 M. D. Defuria, M. Zeller and D. T. Genna, *Cryst. Growth Des.*, 2016, **16**, 3530–3534.

161 P. W. Seo, B. N. Bhadra, I. Ahmed, N. A. Khan and S. H. Jhung, *Sci. Rep.*, 2016, **6**, 1–11.

162 N. Fathma and Y.-K. Jeong, *Int. J. Plant, Anim. Environ. Sci.*, 2019, **9**, 63–73.

163 M. V. Paula, A. L. Barros, K. A. Wanderley, G. F. De Sá, M. Eberlin, T. A. Soares and S. A. Alves, *J. Braz. Chem. Soc.*, 2018, **29**, 2127–2136.

164 S. Lin, Y. Zhao and Y. S. Yun, *ACS Appl. Mater. Interfaces*, 2018, **10**, 28076–28085.

165 D. T. C. Nguyen, H. T. N. Le, T. S. Do, V. T. Pham, D. L. Tran, V. T. T. Ho, T. Van Tran, D. C. Nguyen, T. D. Nguyen, L. G. Bach, H. K. P. Ha and V. T. Doan, *J. Chem.*, 2019, 5602957.

166 S. Kim, J. C. Muñoz-Senmache, B.-M. Jun, C. M. Park, A. Jang, M. Yu, A. J. Hernández-Maldonado and Y. Yoon, *Chem. Eng. J.*, 2020, **382**, 122920.

167 N. Fathma and Y.-K. Jeong, *Int. J. Plant, Anim. Environ. Sci.*, 2019, **9**, 63–73.

168 A. M. Omer, E. M. Abd El-Monaem, G. M. El-Subruiti, M. M. Abd El-Latif and A. S. Eltaweil, *Sci. Rep.*, 2021, **11**, 23818.

169 A. Chatterjee, A. K. Jana and J. K. Basu, *New J. Chem.*, 2021, **45**, 17196–17210.

170 M. S. Samuel, K. Venkatesan Savunthari, N. Chandrasekar, R. Balaji and E. Selvarajan, *Environ. Technol. Innovation*, 2022, **25**, 102216.

171 N. F. Tumpa and Y.-K. Jeong, *Asian Rev. Environ. Earth Sci.*, 2018, **5**, 1–7.

172 S. Gautam, H. Agrawal, M. Thakur, A. Akbari, H. Sharda, R. Kaur and M. Amini, *J. Environ. Chem. Eng.*, 2020, **8**, 103726.

173 M. Wen, G. Li, H. Liu, J. Chen, T. An and H. Yamashita, *Environ. Sci.: Nano*, 2019, **6**, 1006–1025.

174 M. B. Ahmed, J. L. Zhou, H. H. Ngo, W. Guo, N. S. Thomaidis and J. Xu, *J. Hazard. Mater.*, 2017, **323**, 274–298.

175 U. G. Akpan and B. H. Hameed, *J. Hazard. Mater.*, 2009, **170**, 520–529.

176 T. An, L. Sun, G. Li, Y. Gao and G. Ying, *Appl. Catal., B*, 2011, **102**, 140–146.

177 N. Daneshvar, D. Salari and A. R. Khataee, *J. Photochem. Photobiol., A*, 2004, **162**, 317–322.

178 S. C. Yan, Z. S. Li and Z. G. Zou, *Langmuir*, 2009, **25**, 10397–10401.

179 X. Zhang, J. Wang, X.-X. Dong and Y.-K. Lv, *Chemosphere*, 2020, **242**, 125144.

180 H. Kaur, A. Kumar, R. R. Koner and V. Krishnan, in *Nano-Materials as Photocatalysts for Degradation of Environmental Pollutants*, ed. P. Singh, A. Borthakur, P. K. Mishra and D. Tiwary, Elsevier, 2020, pp. 91–126.

181 P. D. Du, H. T. M. Thanh, T. C. To, H. S. Thang, M. X. Tinh, T. N. Tuyen, T. T. Hoa and D. Q. Khieu, *J. Nanomater.*, 2019, **2019**, 6061275.

182 N. Serpone and A. V. Emeline, *J. Phys. Chem. Lett.*, 2012, **3**, 673–677.

183 J. Qiu, X. Zhang, Y. Feng, X. Zhang, H. Wang and J. Yao, *Appl. Catal., B*, 2018, **231**, 317–342.

184 K. G. M. Laurier, F. Vermoortele, R. Ameloot, D. E. De Vos, J. Hofkens and M. B. J. Roeffaers, *J. Am. Chem. Soc.*, 2013, **135**, 14488–14491.

185 M. A. Nasalevich, M. Van Der Veen, F. Kapteijn and J. Gascon, *CrystEngComm*, 2014, **16**, 4919–4926.

186 M. Gheytanzadeh, A. Baghban, S. Habibzadeh, K. Jabbour, A. Esmaeili, A. Mohaddespour and O. Abida, *Sci. Rep.*, 2022, **12**, 1–11.

187 Z. Zhang, X. Li, B. Liu, Q. Zhao and G. Chen, *RSC Adv.*, 2016, **6**, 4289–4295.

188 X. Li, Z. Le, X. Chen, Z. Li, W. Wang, X. Liu, A. Wu, P. Xu and D. Zhang, *Appl. Catal., B*, 2018, **236**, 501–508.

189 P. Yao, H. Liu, D. Wang, J. Chen, G. Li and T. An, *J. Colloid Interface Sci.*, 2018, **522**, 174–182.

190 L. Wen, J. Zhao, K. Lv, Y. Wu, K. Deng, X. Leng and D. Li, *Cryst. Growth Des.*, 2012, **12**, 1603–1612.

191 L. Sondermann, W. Jiang, M. Shviro, A. Spieß, D. Woschko, L. Rademacher and C. Janiak, *Molecules*, 2022, **27**(4), 1241.

192 P. Mahata, G. Madras and S. Natarajan, *J. Phys. Chem. B*, 2006, **110**, 13759–13768.

193 J. Panda, S. N. Sahu, R. R. Tripathy, T. Sahoo, J. R. Sahu, S. K. Pattanayak and R. Sahu, *Photocatal. Degrad. Dyes*, 2021, 489–508.

194 G. Ramalingam, R. Pachaiappan, P. S. Kumar, S. Dharani, S. Rajendran, D. V. N. Vo and T. K. A. Hoang, *Chemosphere*, 2022, **288**, 132448.

195 H. Li, M. Eddaoudi, M. O'Keeffe and O. M. Yaghi, *Nature*, 1999, **402**, 276–279.

196 M. Alvaro, E. Carbonell, B. Ferrer, F. X. Llabrés I Xamena and H. Garcia, *Chem.–Eur. J.*, 2007, **13**, 5106–5112.

197 X. Chen, Y. Chen, Z. Xia, H. Hu, Y. Sun and W. Huang, *Dalton Trans.*, 2012, **41**, 10035–10042.

198 M. C. Das, H. Xu, Z. Wang, G. Srinivas, W. Zhou, Y. F. Yue, V. N. Nesterov, G. Qian and B. Chen, *Chem. Commun.*, 2011, **47**, 11715–11717.

199 L. Á. Alfonso Herrera, P. K. Camarillo Reyes, A. M. Huerta Flores, L. T. Martínez and J. M. Rivera Villanueva, *Mater. Sci. Semicond. Process.*, 2020, **109**, 104950.

200 Y. Gong, P. G. Jiang, Y. X. Wang, T. Wu and J. H. Lin, *Dalton Trans.*, 2013, **42**, 7196–7203.

201 M. Zhang, M. Bosch, T. Gentle and H. C. Zhou, *CrystEngComm*, 2014, **16**, 4069–4083.

202 H. Kaur, M. Venkateswarulu, S. Kumar, V. Krishnan and R. R. Koner, *Dalton Trans.*, 2018, **47**, 1488–1497.

203 H. Kaur, R. Kumar, A. Kumar, V. Krishnan and R. R. Koner, *Dalton Trans.*, 2019, **48**, 915–927.

204 H. Zhao, Y. Zhao, X. Zhao and D. Liu, *J. Mol. Struct.*, 2022, **1263**, 133121.

205 S. Liu, Q. Zou, Y. Ma, D. Chi, R. Chen, H. Fang, W. Hu, K. Zhang and L. F. Chen, *Inorg. Chim. Acta*, 2022, **536**, 120918.

206 C. Wang, H. Jing and P. Wang, *J. Mol. Struct.*, 2014, **1074**, 92–99.

207 S. Rojas-Buzo, P. García-García and A. Corma, *Green Chem.*, 2018, **20**, 3081–3091.

208 B.-H. Wang, X. Lian and B. Yan, *Talanta*, 2020, **214**, 120856.

209 O. M. Yaghi, G. Li and H. Li, *Nature*, 1995, **378**, 703–706.

210 X. Fang, B. Zong and S. Mao, *Nano-Micro Lett.*, 2018, **10**, 64.

211 J. Zhang, Y. Huang, D. Yue, Y. Cui, Y. Yang and G. Qian, *J. Mater. Chem. B*, 2018, **6**, 5174–5180.

212 Y. N. Zeng, H. Q. Zheng, X. H. He, G. J. Cao, B. Wang, K. Wu and Z. J. Lin, *Dalton Trans.*, 2020, **49**, 9680–9687.

213 P. Samanta, S. Let, W. Mandal, S. Dutta and S. K. Ghosh, *Inorg. Chem. Front.*, 2020, **7**, 1801–1821.

214 X. J. Zhang, F. Z. Su, D. M. Chen, Y. Peng, W. Y. Guo, C. S. Liu and M. Du, *Dalton Trans.*, 2019, **48**, 1843–1849.

215 X. Wang, M. Lei, T. Zhang, Q. Zhang, R. Zhang and M. Yang, *Dalton Trans.*, 2021, **50**, 3816–3824.

216 Z. J. Lin, H. Q. Zheng, H. Y. Zheng, L. P. Lin, Q. Xin and R. Cao, *Inorg. Chem.*, 2017, **56**, 14178–14188.

217 Y. B. Lu, Y. Q. Liao, L. Dong, S. D. Zhu, H. R. Wen, J. Huang, X. X. Dai, P. Lian, X. M. Jiang, R. Li and Y. R. Xie, *Chem. Mater.*, 2021, **33**, 7858–7868.

218 Y. X. Sun, G. Guo, W. M. Ding, W. Y. Han, J. Li and Z. P. Deng, *CrystEngComm*, 2022, **24**(7), 1358–1367.

219 M. Gutiérrez, A. F. Möslein and J. C. Tan, *ACS Appl. Mater. Interfaces*, 2021, **13**(6), 7801–7811.

220 E. Moradi, R. Rahimi and V. Safarifard, *J. Solid State Chem.*, 2020, **286**, 121277.

221 Y.-P. Li, X.-H. Zhu, S.-N. Li, Y.-C. Jiang, M.-C. Hu and Q.-G. Zhai, *ACS Appl. Mater. Interfaces*, 2019, **11**, 11338–11348.

222 X.-M. Tian, S.-L. Yao, C.-Q. Qiu, T.-F. Zheng, Y.-Q. Chen, H. Huang, J.-L. Chen, S.-J. Liu and H.-R. Wen, *Inorg. Chem.*, 2020, **59**, 2803–2810.

223 Y. Yu, Y. Wang, H. Yan, J. Lu, H. Liu, Y. Li, S. Wang, D. Li, J. Dou, L. Yang and Z. Zhou, *Inorg. Chem.*, 2020, **59**, 3828–3837.

224 S. Fajal, P. Samanta, S. Dutta and S. K. Ghosh, *Inorg. Chim. Acta*, 2020, **502**, 119359.

225 S. Dutta, S. Let, M. M. Shirolkar, A. V. Desai, P. Samanta, S. Fajal, Y. D. More and S. K. Ghosh, *Dalton Trans.*, 2021, **50**, 10133–10141.

226 H. Min, Z. Han, M. Wang, Y. Li, T. Zhou, W. Shi and P. Cheng, *Inorg. Chem. Front.*, 2020, **7**, 3379–3385.

227 Y. N. Zeng, H. Q. Zheng, J. F. Gu, G. J. Cao, W. E. Zhuang, J. di Lin, R. Cao and Z. J. Lin, *Inorg. Chem.*, 2019, **58**, 13360–13369.

228 L. Li, J. Y. Zou, L. Zhang, S. Y. You, X. Xie and G. H. Chen, *J. Solid State Chem.*, 2022, **305**, 122668.

229 L. Fan, F. Wang, D. Zhao, Y. Peng, Y. Deng, Y. Luo and X. Zhang, *Appl. Organomet. Chem.*, 2020, **34**(12), e5960.

230 K. Ren, S.-H. Wu, X.-F. Guo and H. Wang, *Inorg. Chem.*, 2019, **58**, 4223–4229.

231 H. Wang, D. Liu, M. Wei, W. Qi, X. Li and Y. Niu, *Environ. Res.*, 2022, **208**, 112652.

232 M. Lei, F. Ge, X. Gao, Z. Shi and H. Zheng, *Inorg. Chem.*, 2021, **60**, 10513–10521.

233 S. Singh, A. Numan, Y. Zhan, V. Singh, T. Van Hung and N. D. Nam, *J. Hazard. Mater.*, 2020, **399**, 123042.

234 S. Safaei, J. Wang and P. C. Junk, *J. Solid State Chem.*, 2021, **294**, 121762.

235 S. Wu, H. Min, W. Shi and P. Cheng, *Adv. Mater.*, 2019, **32**(3), 1805871.

236 N. Kajal, V. Singh, R. Gupta and S. Gautam, *Environ. Res.*, 2022, **204**, 112320.

237 Y. Xu, Q. Li, H. Xue and H. Pang, *Coord. Chem. Rev.*, 2018, **376**, 292–318.

238 Y. Xue, S. Zheng, H. Xue and H. Pang, *J. Mater. Chem. A*, 2019, **7**, 7301–7327.

239 C.-S. Liu, J. Li and H. Pang, *Coord. Chem. Rev.*, 2020, **410**, 213222.

240 S. S. Ming, N. S. K. Gowthaman, H. N. Lim, P. Arul, E. Narayanamoorthi, I. Ibrahim, H. Jaafar and S. A. John, *J. Electroanal. Chem.*, 2021, **883**, 115067.

241 W. Ye, Y. Li, J. Wang, B. Li, Y. Cui, Y. Yang and G. Qian, *J. Solid State Chem.*, 2020, **281**, 121032.

242 M. Lu, Y. Deng, Y. Luo, J. Lv, T. Li, J. Xu, S. Chen and J. Wang, *Anal. Chem.*, 2018, **91**, 888–895.

243 M. Baghayeri, M. Ghanei-Motlagh, R. Tayebee, M. Fayazi and F. Narenji, *Anal. Chim. Acta*, 2020, **1099**, 60–67.

244 X. Wang, Y. Qi, Y. Shen, Y. Yuan, L. Zhang, C. Zhang and Y. Sun, *Sens. Actuators, B*, 2020, **310**, 127756.

245 Q. Tian, J. Xu, Y. Zuo, Y. Li, J. Zhang, Y. Zhou, X. Duan, L. Lu, H. Jia, Q. Xu and Y. Yu, *J. Electroanal. Chem.*, 2019, **837**, 1–9.

246 M. B. Nguyen, V. T. Hong Nhung, V. T. Thu, D. T. Ngoc Nga, T. N. Pham Truong, H. T. Giang, P. T. Hai Yen, P. H. Phong, T. A. Vu and V. T. Thu Ha, *RSC Adv.*, 2020, **10**, 42212–42220.

247 M. B. Nguyen, V. T. Hong Nhung, V. T. Thu, D. T. Ngoc Nga, T. N. Pham Truong, H. T. Giang, P. T. Hai Yen, P. H. Phong, T. A. Vu and V. T. Thu Ha, *RSC Adv.*, 2020, **10**, 42212–42220.

248 Z. Zeng, X. Fang, W. Miao, Y. Liu, T. Maiyalagan and S. Mao, *ACS Sens.*, 2019, **4**, 1934–1941.

249 C. Zhao, Y. Fujii, J. Yan, K. H. Harada and A. Koizumi, *Chemosphere*, 2015, **119**, 711–718.

250 X. Zhao, J. Bai, X. Bo and L. Guo, *Anal. Chim. Acta*, 2019, **1075**, 71–80.

251 X. Fang, X. Chen, Y. Liu, Q. Li, Z. Zeng, T. Maiyalagan and S. Mao, *ACS Appl. Nano Mater.*, 2019, **2**, 2367–2376.

252 J. Chen, J. Pan and S. Chen, *Chem. Commun.*, 2017, **53**, 10224–10227.

253 Y. Yu, X. M. Zhang, J. P. Ma, Q. K. Liu, P. Wang and Y. bin Dong, *Chem. Commun.*, 2014, **50**, 1444–1446.

254 Y. Wang, M. Zhao, C. Hou, X. Yang, Z. Li, Q. Meng and C. Liang, *J. Taiwan Inst. Chem. Eng.*, 2019, **102**, 312–320.

255 X. Qi, H. Tian, X. Dang, Y. Fan, Y. Zhang and H. Zhao, *Anal. Methods*, 2019, **11**, 1111–1124.

256 Z. Wang, J. Yang, Y. Li, Q. Zhuang and J. Gu, *Dalton Trans.*, 2018, **47**, 5570–5574.

257 H. Lai, G. Li, F. Xu and Z. Zhang, *J. Mater. Chem. C*, 2020, **8**, 2952–2963.

258 T. Yu, C. Ho, C. Wu and C. Chien, *J. Raman Spectrosc.*, 2013, 1506–1511.

259 P. Falcaro, R. Ricco, A. Yazdi, I. Imaz, S. Furukawa, D. Maspoch, R. Ameloot, J. D. Evans and C. J. Doonan, *Coord. Chem. Rev.*, 2016, **307**, 237–254.

260 Y. Hu, J. Liao, D. Wang and G. Li, *Anal. Chem.*, 2014, **86**(8), 3955–3963.

261 T. Xuan, Y. Gao, Y. Cai, X. Guo, Y. Wen and H. Yang, *Sens. Actuators, B*, 2019, **293**, 289–295.

262 O. Guselnikova, P. Postnikov, R. Elashnikov, E. Miliutina, V. Svorcik and O. Lyutakov, *Anal. Chim. Acta*, 2019, **1068**, 70–79.

263 X. Cao, S. Hong, Z. Jiang, Y. She, S. Wang, C. Zhang, H. Li, F. Jin, M. Jin and J. Wang, *Analyst*, 2017, **142**, 2640–2647.

264 D. Li, X. Cao, Q. Zhang, X. Ren, L. Jiang, D. Li, W. Deng and H. Liu, *J. Mater. Chem. A*, 2019, **2019**(7), 14108–14117.

265 H. Lai, W. Shang, Y. Yun, D. Chen and L. Wu, *Microchim. Acta*, 2019, **186**, 144.

266 X. Ma, H. Liu, S. Wen, Q. Xie, L. Li, J. Jin, X. Wang, B. Zhao and W. Song, *Nanotechnology*, 2020, **31**, 315501.

267 G. Jiang, Z. Wang, S. Zong, K. Yang, K. Zhu and Y. Cui, *J. Hazard. Mater.*, 2021, **408**, 124426.